A MICROMECHNICS APPROACH TO PREDICTING THE ONSET YIELDING ENVELOPE OF PARTICULATE COMPOSITE MATERIALS

by

BEHROOZ KARIMI

Presented to the Faculty of the Graduate School of

The University of Texas at Arlington in Partial Fulfillment

of the Requirements

for the Degree of

DOCTOR OF PHILOSOPHY

THE UNIVERSITY OF TEXAS AT ARLINGTON

December 2017

Acknowledgment

I would like to thank my supervising professor, Dr. Seiichi Nomura, for his continuous support and help throughout my doctoral work. Without his persistent help, this dissertation would have taken much more time. I would also like to express my gratitude to the members of my dissertation committee for their willingness in reviewing and evaluating this work.

My father and mother deserve a special mention for their continual support throughout my studies. Many thanks to my siblings especially, Omid, for their patience and understanding which is invaluable.

December 11, 2017

Abstract

A MICROMECHNICS APPROACH TO PREDICTING THE ONSET YIELDING ENVELOPE OF PARTICULATE COMPOSITE MATERIALS

Behrooz Karimi, Ph.D

The University of Texas at Arlington, 2017

Supervising Professor: Seiichi Nomura

Composite materials fail for various reasons and extensive research has been conducted both experimentally and theoretically. However, theoretical prediction of composite failure by yielding seems scarce. Adding reinforcing elements to matrix significantly affects the structural behavior of composite materials. The inserted particles on one hand obstruct the progress of cracks and on the other hand cause stress concentration on the interface of the particle-matrix and eventually influence the ultimate strength of the material. In this research, we study the interface stresses and strength in particulate reinforced composites under uniform mechanical and thermal loading. We theoretically obtain failure envelopes for particulate reinforced composites. This is achieved by estimating the stress field in the matrix phase around a spheroidal particle in an unbounded matrix phase along with the self-consistent approximation that determines the effective elastic modulus of the composite. The failure envelopes are calculated on the basis of the maximum von Mises stress as a function of the applied far-field stresses or heat flow. We also discuss the effect of the particle volume fractions and the particle to matrix stiffness ratios on the interface stresses and ultimate yielding strength. Parametric analysis enables us to predict these envelopes for various loading conditions, volume fractions and particle to matrix stiffness ratios.

Table of Contents

List of illustrations

List of Tables

Chapter 1

Introduction

Particulate composite materials are becoming increasingly advantageous in manufacturing products for military and everyday applications. Composite materials are now utilized in many application fields ranging from sporting to automobile to military and aerospace industries. Composites are available in many forms but they always consist of two main elements: the matrix and reinforcing elements with different mechanical and thermal properties from the matrix. The reinforcing elements could be particles, short fibers or continuous fibers which have different diameters and length to diameter ratios. The continuous fibers are either parallel or woven together in the matrix phase.

Table 1-1 Example of matrix and particles used in industry

Matrix	Aluminum, steel, magnesium
Particle	$Al_2O_3, Alumina$ $B_4C, Boron - Carbide$ $SiC, silicon\ carbide$

Due to the inhomogeneous and anisotropic nature of composite materials, it is difficult to predict their strength prior to manufacturing and testing. The characteristics of composite materials having short fibers are different from the one consisting of continuous fibers. The behavior of a composite material made from parallel fibers is different from the one made from woven form of the same fiber. A change in the volume fraction of the reinforcing element will also change the composite materials behavior and properties. One of the known advantages of composite materials with continuous fibers is the ability to tailor the composite materials properties to meet a specific need. The variability of the fiber volume fractions, ply orientations, stacking sequence and other

parameters brings flexibility in the product design. The same variability of composite materials that makes it useful, also makes it difficult to specify its characteristics without expensive testing.

The well-developed theories for evaluating the strength of composite materials are mainly for composite laminates. Lamination theory is well formulated by Tsai and Wu [1] and developed more in other works such as Christensen [2], Tsai and Hahn [3] and Ashbee [4]. The lamination theory studies the behavior of composites under applied loading in a macroscopic view, i.e. the response of each ply in a laminate is considered altogether and the fiber-matrix interaction is not considered. Since the stress and strain fields inside the ply are not calculated, the only way to determine the onset strain of ply failure is to perform tests and could not be calculated from the matrix and fiber material characteristics.

The micromechanics approach is an alternative way of studying composite materials. This approach tries to determine the strain and stress fields within the fiber and matrix material. It can describe the interaction among the matrix and fibers. In this approach, the type of reinforcing elements could be continuous, spherical, platelet and chopped fibers. Researchers have studied these cases and predicted their behavior. Argon [5], Benveniste and Aboudi [6], Mikata and Taya [7], Taya and Chou [8] as well as Nomura and Oshima [9] have researched a variety of short fiber and spherically reinforced composites and studied the mechanical characteristics of composite materials as well as the strain and stress fields inside the matrix and reinforcing elements.

The stiffness of particulate composites has been studied extensively [10]. The presence of particles inside the matrix material disturbs the stress field. Therefore, they affect the effective properties of the composite materials as a whole. The effective properties are used to predict the mechanical performance of the composite materials.

These effective property estimations could be categorized into two main forms of the upper and lower bounds or the effective property approximation based on the microstructure details of the composite materials. Using the variational principle, Hashin and Shtrikman [11] evaluated the upper and lower bounds for the effective properties of multiphase linear elastic materials. Nemat-Naser [12] extended Hashin's approach to multiphase elastic-plastic materials. The effective property approach tries to evaluate the effective properties of the composite materials exactly. This approach is based on consideration of a representative volume element (RVE) for the homogenization purpose. Budiansky [13] developed a self-consistent (S-C) method scheme. Mori and Tanaka [14] extended the S-C approach. These approaches are based on a single inclusion in an unbounded matrix. Other approaches have considered the interaction among the inclusions such as the three-phase model by Christensen and Lo [15]. Also computational methods such as FEM have been utilized in evaluating the effective properties of composite materials. Zhang and Wu [16] examined the effect of inclusion connectivity on the effective properties. They showed that the inclusion volume fractions and connectivity affect the effective properties significantly. These approaches have been developed in order to account for the inclusion interactions more accurately. The concept of unit cells could also be used. Each unit cell contains a finite number of inclusions and is repeated periodically. This approach gives better description of microstructure details of the composite materials. Paley and Aboudi [17] studied the repeating unit cells through developing the generalized method of cells.

Javier [18] claims that since damage is a local phenomenon, therefore using the average theorems and homogenization techniques is not effective. Damage causes local deformation gradient fields and the average methods are unable to capture the effects from local phenomena. Also using the periodic micro-field approaches is not useful

because they assume damage also periodically progresses throughout the material while in practice that is not the case. Therefore, he proposed the study of microstructure effect on the damage using the finite element method. Sozhamannan [19] used SEM images to find the microstructure of a specific specimen and used FEM to model the fracture process of the particulate reinforced metal matrix composite. He realized that the clustering nature of the particles determines the failure type of the composite materials.

Dong [20] did some experiments to realize the effect of particle size on fracture and debonding. He used a body center cubic system to analyze the elastic energy of the damaged cells. He predicted the tensile strength of the specimens. Kusch [21] used a series solution to get the stress concentration at periodic configuration of particles in transversely isotropic matrix. His results show that the particle volume fraction has a significant effect on the stress concentration around the particles.

One of the purposes of micromechanics of composites is to evaluate the macroscopic composite properties through incorporating microstructural elements. Two major approaches are generally considered, the first is to use homogenization techniques to describe the behavior of a representative volume element and the second is to use a periodic micro-field approach to describe the behavior of a unit cell. Both methods have high computational costs and do not give analytical expressions for the stress fields and composite strength. Birman [22] conducted research on the strength of particulate polymers. He used the analytical stress distribution around spherical particles and extended it using the Mori-Tanaka homogenization approach [23] to get the stress concentrations around the particle, then he used the von Mises and maximum principal stress values to compare the strength of polymers against the matrix yielding and particle to matrix debonding strength.

The micromechanics description of composite materials under applied loading has been carried out using computational and closed form analytical approaches. The finite element method is the dominant computational approach. The closed form mathematical approaches are based on the work of Eshelby [24].

Allowable combined state of stress applied on a composite material has not been investigated yet using the equivalent inclusion approach. This dissertation presents the failure envelope prediction of particulate composite materials using a micromechanics approach. The assumptions made are:

1. The maximum von Mises stress occurs in the matrix adjacent to the fibers.
2. The von Mises failure criterion governs the matrix failure.
3. The fiber shape is ellipsoidal.
4. The composite material is homogeneous as a whole.
5. The reinforcing particles are very small relative to a unit volume of composite materials.

Considering these assumptions in the formulation, we determine the strength of composite materials based on the strength of the matrix and fiber material and other varying parameters of the composite. We account for the anisotropic properties of the composite in the formulation. The developed model herein allows predicting the strength of a variety of composites using the constituent's mechanical properties without a need for expensive tests.

In order to reach the objective of this study, we must find the stress field at the interface of the matrix and fiber in terms of the properties of the matrix and fiber materials as well as the applied loading. Chapter 2 describes the analysis procedure and solution approach. First the composite material is replaced with an equivalent medium having the effective properties of the composite material. After we evaluate the stress inside a

particle embedded in the composite material using Eshelby's method and continuity of the traction and displacement at the particle-matrix interface, then we obtain the stress outside the particle. Using the stress outside the particle where the maximum von Mises stress happens, we obtained and plotted the failure envelopes. We investigated and plotted the effect of various parameters on the stress field and the failure envelopes.

Chapter 3 deals with the thermo-elastic field of a two phase material. We obtain the stress field inside and outside a particle embedded in an isotropic matrix under thermal heat flow at the far-field. Then using the von Mises failure criterion, we obtain and present the failure envelopes due to thermal stresses for popular composite materials used in industry.

Chapter 4 summarizes the dissertation as a whole and elaborates on the important results obtained in this study. Also it presents some ideas for continuation of this research.

Chapter 2

Mechanical Analysis

The interaction among neighboring reinforcing elements makes the process of deriving the stress field inside the matrix almost impossible to implement. The self-consistent (S-C) approximation is used to replace the composite aggregate with an equivalent homogeneous material which possesses the stiffness properties of the composite. This way an isolated reinforcing element embedded in an equivalent medium to the composite materials could be studied. The interaction among adjacent particles is reflected in the response of the combined materials.

The self-consistent (S-C) method is a homogenization approach. Similar to the experimental testing specimen scales, a microscopic volume element is considered as a representative of the entire material. The Representative Volume Element (RVE) is utilized in the homogenization of the material properties to describe the macroscopic properties of composite materials. The evaluated properties should be independent of the location of the volume element. As it will be described more thoroughly in the next following paragraphs, the matrix is replaced with a medium having the S-C approximated properties. Hooke's law takes the following form in the replaced material:

$$\langle \sigma_{ij} \rangle = \bar{C}_{ijkl} \langle \epsilon_{kl} \rangle \tag{2.1}$$

where $\langle \sigma_{ij} \rangle$ and $\langle \epsilon_{kl} \rangle$ are the average stress and strain, respectively and $\bar{C}_{ijkl}$ represents the effective composite material properties.

There are various homogenization approaches and it is worthwhile to briefly explain the differences among these approaches qualitatively, without thorough consideration [25].

The Voigt and Reuss approximation is the simplest form of homogenization. The Voigt method assumes that in the representative volume element, the strain is constant and Reuss assumes that the stress is constant which leads to the following relations for the effective elastic stiffness $\bar{C}$:

$$\bar{C}_{Voigt} = \sum_{\alpha} v_{\alpha} C_{\alpha} \tag{2.2}$$

$$\bar{C}_{Reuss}{}^{-1} = \sum_{\alpha} v_{\alpha} C_{\alpha}{}^{-1} \tag{2.3}$$

where v_{α} and C_{α} are the volume fraction and elasticity tensor of the α-th phase of the composite material, respectively. The Voight approximation is also referred to as the rule of mixture. These methods violate the requirements such as local equilibrium at phase boundaries but provide the upper and lower bounds for the effective properties.

The next approach is called dilute distribution. This method assumes that the particles are so far from each other that their interaction to each other and with the boundaries of the RVE could be neglected. In this case, each particle is considered in an unbounded matrix phase under the applied far-field strain or stress. This case is equivalent to assuming that the same applied far-field strains, ϵ^{∞}, are applied to the RVE embedding only one particle. The formulation of the effective stiffness in dilute distribution condition is explicitly expressed as:

$$\bar{C} = C^M + v_f (C^f - C^M) \left(I + S^M (C^M)^{-1} (C^f - C^M) \right)^{-1} \tag{2.4}$$

The superscripts, *f* and *M,* represent the fiber (particle) and matrix, respectively. The quantity, $\bar{C}$, is the effective elasticity tensor of the composite material. The tensor, S^M, is the Eshelby tensor evaluated using the matrix material properties. The tenosr, I, is an identity tensor.

More advanced methods are the Mori-Tanaka and self-consistent (S-C) methods. The Mori-Tanaka method is similar to the dilute distribution approach with one distinction. This method assumes that the RVE which contains one particle is under the average matrix strain, $\langle\epsilon\rangle_M$, at the boundary while the dilute distribution model RVE was under the strain applied at the far-field, ϵ^∞. Based on this assumption, the effective elastic stiffness is evaluated and expressed as

$$\bar{C} = C^M + v_f(C^f - C^M)\left(I + v_M S^M (C^M)^{-1}(C^f - C^M)\right)^{-1} \tag{2.5}$$

where v_M is the volume fraction of the matrix.

The self-consistent method assumes a very different condition. Just like the dilute distribution method, the applied far-field strain ϵ^∞ is also applied to the RVE with the distinction that the particle is embedded in a medium with the effective properties of the composite material. In this study, we adopted the self-consistent approach and therefore we will explain it more thoroughly than the other approaches. In the following, the S-C approximation is derived.

Hooke's law between the average strain and stress defines the effective elasticity tensor as follows:

$$\langle\sigma_{ij}\rangle = \bar{C}_{ijkl}\langle\epsilon_{kl}\rangle \tag{2.6}$$

where $\langle\sigma_{ij}\rangle$ and $\langle\epsilon_{kl}\rangle$ are the average stress and strain which are equal to the applied stress and strain at the far-field.

The local Hooke's law also must be valid and is expressed as follows:

$$\sigma_{ij}(x) = C_{ijkl}(x)\,\epsilon_{kl}(x) \tag{2.7}$$

Taking average of both sides of Eq. (2.7) and combining with Eq. (2.6) gives

$$\bar{C}_{ijkl}\ \langle\epsilon_{kl}\rangle = \langle C_{ijkl}\,\epsilon_{kl}\rangle \tag{2.8}$$

Since the solution to the linear elastic boundary value problem is unique, therefore, the strain field inside the RVE is a linear function of the loading parameter, ϵ_{ij}^{∞}, as follows:

$$\epsilon_{ij}(x) = A_{ijkl}(x)\,\epsilon_{kl}^{\infty} \tag{2.9}$$

The quantity, $A_{ijkl}(x)$, is called the influence tensor and relates the local strain field, $\epsilon_{ij}(x)$, to the applied strain at the far-field, ϵ_{kl}^{∞}. Inserting Eq. (2.9) into Eq. (2.8) and expanding the resulting relation gives the following expression:

$$\bar{C}_{ijkl}\ \langle\epsilon_{kl}\rangle = \langle C_{ijkl}\,A_{klmn}\rangle\,\epsilon_{mn}^{\infty} \tag{2.10}$$

Based on the average theorem for infinitesimal strain in incompressible material under constant strain ϵ_{ij}^{∞}, we have:

$$\langle\epsilon_{ij}\rangle = \epsilon_{ij}^{\infty} \tag{2.11}$$

The derivation of Eq. (2.11) is as follows: suppose that an RVE is subjected to prescribed displacement boundary condition. On the boundary we have:

$$u_i^0 = \varepsilon_{ij}^{\infty} x_j \tag{2.12}$$

where u_i^0 is the displacement on the surface of the boundary. Taking the average of the strain over the volume of the RVE gives:

$$\langle\epsilon_{ij}\rangle_V = \frac{1}{V}\int_V \epsilon_{ij}\,dV = \frac{1}{2V}\int_V (u_{i,j} + u_{j,i})\,dV = \frac{1}{2V}\oint_{\partial V} (u_i^0 n_j + u_j^0 n_i)dS \tag{2.13}$$

Therefore, substituting Eq. (2.12) into Eq. (2.13) results in:

$$\langle\epsilon_{ij}\rangle_V = \tfrac{1}{2V}\ \oint_{\partial V}(\varepsilon_{ik}^{\infty} x_k n_j + \varepsilon_{jk}^{\infty} x_k n_i)dS = \tfrac{1}{2V}\ \int_V (\varepsilon_{ik}^{\infty}\delta_{kj} + \varepsilon_{jk}^{\infty}\delta_{ki})\,dV = \varepsilon_{ij}^{\infty} \tag{2.14}$$

Therefore, Eq. (2.11) is proved and is used in the following analysis. Combining Eq. (2.11) with Eq. (2.10) gives the following relation:

$$\bar{C}_{ijmn}\ = \langle C_{ijkl}\,A_{klmn}\rangle \tag{2.15}$$

For piecewise constant elastic properties of the material phases, the above relation is simplified to

$$\bar{C}_{ijkl} = \sum_{\alpha} v_{\alpha} C_{\alpha} A_{\alpha} \tag{2.16}$$

Also taking the average of both sides of Eq. (2.9) over the volume of phase α and the whole RVE gives the following two relations:

$$\langle \epsilon \rangle_{\alpha} = \langle A \rangle_{\alpha} \, \epsilon^{\infty} \tag{2.17}$$

$$\langle \epsilon \rangle = \langle A \rangle \, \epsilon^{\infty} \tag{2.18}$$

Using Eqs. (2.17) and (2.18), we derive the following relation:

$$\langle A \rangle = 1 = \sum_{\alpha} v_{\alpha} \langle A \rangle_{\alpha} \tag{2.19}$$

Therefore, in two phase composite materials, only the influence tensor for one of the phases is necessary. Combining Eqs. (2.16) and (2.19) leads to the following relation for the effective properties of the composite material:

$$\bar{C} = C^{M} + v_f (C^{f} - C^{M}) \, A\_f_{\bar{C}} \tag{2.20}$$

where A_f is the influence tensor of the particles or fibers. In case of ellipsoidal particles, the influence tensor is evaluated using the Eshelby tensor as follows:

$$A\_f_{\bar{C}} = \left(I + \bar{S}(\bar{C})^{-1} (C^{f} - \bar{C}) \right)^{-1} \tag{2.21}$$

The Eshelby tensor, $\bar{S}$, is evaluated using the effective properties of the composite material. Equation (2.20) is a set of nonlinear equations in which the only unknowns are elements of the effective stiffness, $\bar{C}$. The solution to Eq. (2.20) for $\bar{C}$ can be obtained numerically by iteration. This formulation followed a general approach and could be used for transversely isotropic fibers and matrix.

The Eshelby tensor is required to solve for the S-C approximated properties of the composite material. The concept and formulation of the Eshelby method will be

explained more thoroughly in the next section but the final formulation for evaluating the Eshelby tensor is printed here. Having a transversely isotropic material as the matrix phase, the Eshelby tensor, S_{ikmn}, takes the following form [26]

$$S_{ikmn} = \frac{1}{8\pi} C_{jlmn}(A_{ikjl} + A_{kijl}) \tag{2.22}$$

where C_{jlmn} is the elastic stiffness tensor of the transversely isotropic matrix. Non-zero components of A_{ikjl} are expressed as [27]:

$$C_{11} = d \tag{2.23}$$

$$\frac{C_{11} - C_{12}}{2} = e \tag{2.24}$$

$$C_{44} = f \tag{2.25}$$

$$C_{13} + C_{44} = g \tag{2.26}$$

$$C_{33} = h \tag{2.27}$$

$$A_{1111} = \frac{\pi}{2}\int_0^1 \Delta(1-x^2)\Big((f(1-x^2) + h\rho^2x^2)\big((3e+d)(1-x^2) + 4f\rho^2x^2\big) - g^2\rho^2x^2(1-x^2)\Big)dx \tag{2.28}$$

$$A_{2222} = A_{1111} \tag{2.29}$$

$$A_{2211} = A_{1122} \tag{2.30}$$

$$A_{1122} = \frac{\pi}{2}\int_0^1 \Delta(1-x^2)^2\big(g^2\rho^2x^2 - (d-e)(f(1-x^2) + h\rho^2x^2)\big)dx \tag{2.31}$$

$$A_{3333} = 4\pi\int_0^1 \Delta\rho^2x^2(d(1-x^2) + f\rho^2x^2)(e(1-x^2) + f\rho^2x^2)dx \tag{2.32}$$

$$A_{1212} = A_{2121} = \frac{\pi}{2}\int_0^1 \Delta(1 - x^2)\Big((f(1-x^2) + h\rho^2x^2)\big((e+3d)(1-x^2) + 4f\rho^2x^2\big) - 3g^2\rho^2x^2(1-x^2)\Big)dx \tag{2.33}$$

$$A_{1313} = A_{2323} = 2\pi\int_0^1 \Delta\rho^2x^2\left(((d+e)(1-x^2) + 2f\rho^2x^2)(f(1-x^2) + h\rho^2x^2) - g^2\rho^2x^2(1-x^2)\right)dx \tag{2.34}$$

$$A_{3131} = A_{3232} = 2\pi\int_0^1 \Delta(1 - x^2)\big((d(1-x^2) + f\rho^2x^2)(e(1-x^2) + f\rho^2x^2)\big)dx \tag{2.35}$$

$$A_{1133} = A_{2233} = -2\pi\int_0^1 \Delta g\rho^2x^2(1-x^2)(e(1-x^2) + f\rho^2x^2)dx \tag{2.36}$$

$$\Delta^{-1} = (e(1-x^2) + f\rho^2x^2)\big((d(1-x^2) + f\rho^2x^2)(f(1-x^2) + h\rho^2x^2) - g^2\rho^2x^2(1-x^2)\big) \tag{2.37}$$

So using the components of A_{ijkl} and Eq. (2.22), the Eshelby tensor is obtained. The expressions for A_{ijkl} are to be numerically evaluated and, to the knowledge of the author, explicit symbolic relations are not possible.

2.1 The equivalent inclusion

Now that the matrix properties are replaced with the S-C approximated properties of the composite material, it is time to evaluate the stress inside the particles. The idea of equivalent inclusion will be described here. Eshelby introduced this concept, which states that the mechanical response of an unbounded elastic medium with an embedded

eigenstrain under an applied loading is identical to the behavior of an unbounded elastic medium embedding an inhomogeneity. Modeling composite materials is divided into several steps, describing the response of an inhomogeneity inside an unbounded elastic medium is the first step to proceed. The required equations to calculate the eigenstrain are described here. The stress field within and outside the particle will be expressed in terms of the eigenstrain expressions.

The concept which Eshelby studied is that of an unbounded elastic matrix phase containing an ellipsoidal region with an eigenstrain within it. The eigenstrains are termed stress free strains in the literature [28]. Hooke's law governs the stress-strain relation inside the matrix remote from the pre-strained volume.

$$\sigma_{ij}^{\infty} = \bar{C}_{ijkl}\epsilon_{kl}^{\infty} \tag{2.38}$$

where the quantity, $\bar{C}_{ijkl}$, is the elastic stiffness of the equivalent matrix, σ_{ij}^{∞} is the far-field stress, ϵ_{kl}^{∞} is the far-field strain and subscripts "*k*" and "*l*" are repeated indices in the Einstein notation.

The eigenstrain inside the matrix disturbs the strain and stress field which are represented by ϵ_{ij}^{d} and σ_{ij}^{d}, respectively. The stress field around the pre-strained region due to the applied far-field stress, σ_{ij}^{∞}, is as follows:

$$\sigma_{ij}^{\infty} + \sigma_{ij}^{d} = \bar{C}_{ijkl}(\epsilon_{kl}^{\infty} + \epsilon_{kl}^{d}) \tag{2.39}$$

where the quantity, ϵ_{kl}^{∞}, is the far-field strain and ϵ_{ij}^{d} is the disturbed strain. The stress field within the inclusion is

$$\sigma_{ij}^{\infty} + \sigma_{ij}^{d} = \bar{C}_{ijkl}(\epsilon_{kl}^{\infty} + \epsilon_{kl}^{d} - \epsilon_{kl}^{*}) \tag{2.40}$$

where the tensor,ϵ_{kl}^{*}, is the eigenstrain. Eshelby showed that the strain disturbance, ϵ_{ij}^{d}, could be obtained in terms of the eigenstrain and a quantity known as the Eshelby tensor:

$$\epsilon_{ij}^{d} = \bar{S}_{ijkl}\epsilon_{kl}^{*} \tag{2.41}$$

The Eshelby tensor, $\bar{S}_{ijkl}$, is in terms of the shape of the inclusion and the surrounding medium properties. The Eshelby tensor for an ellipsoidal inclusion is formulated in the literature and is well-known. An ellipsoid could describe a number of common reinforcing elements such as short fibers, long fibers of circular cross section and spherical shapes.

The objective is to formulate the stress field around a particle inside a matrix with different material properties from the matrix in terms of the Eshelby tensor and material properties of the phases. The equivalent inclusion method attempts to find an inclusion with a proper eigenstrain inside a matrix which as a whole would respond to the applied far-field loading exactly the same way as an actual inhomogeneity inside the matrix would. To find such an eigenstrain, the stresses in the actual inclusion are equated to those in a region of matrix embedding the eigenstrain, ϵ_{kl}^{*}, as follows:

$$C_{ijkl}^{f}\left(\epsilon_{kl}^{\infty}+\epsilon_{ij}^{d}\right)=\bar{C}_{ijkl}(\epsilon_{kl}^{\infty}+\epsilon_{kl}^{d}-\epsilon_{kl}^{*}) \tag{2.42}$$

The quantities, C_{ijkl}^{f} and $\bar{C}_{ijkl}$, are the elasticity tensors of the actual inhomogeneity and S-C approximation of the composite material properties, respectively. Substituting the strain disturbance given in Eq. (2.41) into the above expression gives the following:

$$C_{ijkl}^{f}(\epsilon_{kl}^{\infty}+\bar{S}_{klmn}\,\epsilon_{mn}^{*})=\bar{C}_{ijkl}(\epsilon_{kl}^{\infty}+\bar{S}_{klmn}\,\epsilon_{mn}^{*}-\epsilon_{kl}^{*}) \tag{2.43}$$

In the equation above, the effective material properties of the matrix, $\bar{C}_{ijkl}$, the material properties of the actual inhomogeneity, C_{ijkl}^{f}, the far-field strain, ϵ_{kl}^{∞}, and the Eshelby tensor are known. Therefore, it results in a system of linear equations which provides the eigenstrain, ϵ_{mn}^{*}. Consequently, the eigenstrain values will be expressed in terms of the aforementioned known parameters. The explicit form of the eigenstrain in

transversely isotropic matrix is very complex and could not be printed here. In later sections, the eigenstrain for the special case of isotropic material is shown.

Having evaluated the eigenstrain, ϵ_{kl}^{*}, we obtain the stress and strain fields inside the particles in terms of the eigenstrain as:

$$\epsilon_{kl}^{in} = \epsilon_{kl}^{\infty} + S_{klmn}\epsilon_{mn}^{*} \tag{2.44}$$

$$\sigma_{ij}^{in} = C_{ijkl}^{f}(\epsilon_{kl}^{\infty} + \bar{S}_{klmn}\,\epsilon_{mn}^{*}) \tag{2.45}$$

2.2 Stress outside the particle

To calculate the stress outside the particles based on the stress inside the particles, we utilize the continuity conditions for the traction and displacement across the particle-matrix interface; that is [29],

$$[[\, u_i^d \,]] = u_{\mathrm{i}}^{\mathrm{out}} - u_{\mathrm{i}}^{\mathrm{in}} = 0 \tag{2.46}$$

The jump in stress field is formulated as follows:

$$\sigma_{ij}^{out} = \bar{C}_{ijkl}(\epsilon_{kl}^{\infty} + \epsilon_{kl}^{d}) = \sigma_{ij}^{\infty} + \sigma_{ij}^{d} \tag{2.47}$$

$$\sigma_{ij}^{in} = \bar{C}_{ijkl}(\epsilon_{kl}^{\infty} + \epsilon_{kl}^{d} - \epsilon_{kl}^{*}) = \sigma_{ij}^{\infty} + \sigma_{ij}^{d} - \sigma_{ij}^{*} \tag{2.48}$$

Subtracting Eq. (2.48) from Eq. (2.47) results in:

$$[[\, \sigma_{ij} \,]] = \left[\left[\sigma_{ij}^{d}\right]\right] + \sigma_{ij}^{*} \tag{2.49}$$

The bracketed quantity $[[\, f \,]]$ is the jump of field "*f*" from inside of the particle to the outside where "*f*" can be displacement, u_i, stress, σ_{ij}, and strain, ϵ_{ij}. The quantities, $u_{\mathrm{i}}^{\mathrm{out}}$ and $u_{\mathrm{i}}^{\mathrm{in}}$, are the displacements outside and inside the particle-matrix interface, respectively. The quantity, u_i^c, is the disturbed displacement, n_i is the outward unit vector normal to the surface of the particle. The quantity, σ_{ij}^{*} and σ_{ij}^{d}, are the eigenstress inside the inclusion and the disturbed stress, respectively. In this context eigenstress is defined as, $\sigma_{ij}^{*} = \bar{C}_{ijkl}\,\epsilon_{kl}^{*}$.

:

Multiplying Eq. (2.49) by the unit normal vector n_i, results in:

$$[[\,\sigma_{ij}\,n_i]] = \left[\left[\sigma_{ij}^{d}\right]\right] n_i + \sigma_{ij}^{*} n_i \tag{2.50}$$

the vector, $[[\,\sigma_{ij}\,n_i]]$, is the jump of the traction on the interface which is equated to zero as follows:

$$\left[\left[\sigma_{ij}^{d}\,\right]\right] n_i = -\sigma_{ij}^{*} n_i \tag{2.51}$$

The strain is discontinuous at the particle-matrix interface. The directional differentiation of the displacement along the tangent of the interface must be continuous, therefore, the jump of the displacement derivative must be in the direction of the normal to the interface. The following relation describes the jump parameter of the displacement across the interface:

$$\left[\left[u_{i,j}^{d}\;t_i\right]\right] = 0 \tag{2.52}$$

$$[[u_{i,j}^{d}]] = u_{i,j}^{out} - u_{i,j}^{in} = \lambda_i n_j \tag{2.53}$$

where t_i is the vector tangent to the particle-matrix interface.

$$\left[\left[\epsilon_{ij}^{d}\,\right]\right] = [[\frac{u_{k,l}^{d} + u_{l,k}^{d}}{2}\,]] \tag{2.54}$$

The quantity, C_{ijkl}^{m}, has minor symmetry, therefore, $C_{ijkl}^{m} u_{k,l}^{c} = C_{ijkl}^{m} u_{l,k}^{c}$. Using the minor symmetry of the matrix stiffness along with Eqs. (2.51) and (2.54) gives the following relation:

$$\left[\left[\sigma_{ij}^{d}\,\right]\right] = \bar{C}_{ijkl}\,[[\,u_{k,l}^{d}]] \tag{2.55}$$

Combining Eqs. (2.51), (2.52) and (2.55) gives:

$$\left[\left[\sigma_{ij}^{d}\,\right]\right] n_i = \;\bar{C}_{ijkl}\lambda_k\, n_l\, n_i = -\sigma_{ij}^{*} n_i \tag{2.56}$$

where λ_i is the magnitude of the jump. Equation (2.56) is a set of 3 linear equations in which λ_k is to be determined. In general anisotropic cases, obtaining the explicit relation

for the jump parameter, λ_k, leads to a very long relation, therefore, the resulted relation is not printed here.

Combining Eqs. (2.49) and (2.56) gives the following relation for the stress jump across the interface.

$$\left[\left[\sigma_{ij}\right]\right] = \left[\left[\sigma_{ij}^{d}\right]\right] + \sigma_{ij}^{*} = \sigma_{ij}^{*} - \bar{C}_{ijkl}\lambda_k\, n_l \tag{2.57}$$

Having solved for the jump parameter, the stress outside the particle is evaluated using Eq. (2.57) as follows:

$$\sigma_{ij}^{out} = \sigma_{ij}^{in} + \sigma_{ij}^{*} + \left[\left[\sigma_{ij}^{d}\right]\right] = \bar{C}_{ijkl}(\epsilon_{kl}^{\infty} + \bar{S}_{klmn}\,\epsilon_{mn}^{*}) - \bar{C}_{ijkl}\lambda_k\, n_l \tag{2.58}$$

2.3 Special case: isotropic material and spherical particles

In case of isotropic material properties, the S-C approximation of the composite material properties could be evaluated in a more straightforward approach than the one described in the previous section. Consider spherical particles inside an unbounded isotropic matrix phase. Since the particles are spherical, the effective properties of the composite material would also be isotropic, therefore, only two parameters are necessary to determine the effective elasticity tensor of the composite material. Under uniform shear stress at the far-field, σ_{12}^{∞}, Hooke's law states

$$\sigma_{12}^{\infty} = 2\bar{\mu}\epsilon_{12}^{\infty} \tag{2.59}$$

where the quantity, σ_{12}^{∞}, is the applied far-field shear stress, ϵ_{12}^{∞} is the resulting shear strain in the homogeneous material and $\bar{\mu}$ is the effective shear modulus of the composite material. Based on the equivalent inclusion equation, the stress inside the particle is equated to the stress inside the effective material properties embedding an eigenstrain ϵ_{12}^{*}.

$$\sigma_{12}^{\infty} + \sigma_{12}^{d} = 2\bar{\mu}(\epsilon_{12}^{\infty} + \epsilon_{12}^{d} - \epsilon_{12}^{*}) = 2\mu_f(\epsilon_{12}^{\infty} + \epsilon_{12}^{d}) \tag{2.60}$$

where μ_f is the shear modulus of the particle. The disturbed part of the shear strain, ϵ_{12}^d, is as follows:

$$\epsilon_{12}^d = 2\bar{S}_{1212}\,\epsilon_{12}^* \tag{2.61}$$

The quantity, $\bar{S}_{1212}$, is an element in the Eshelby tensor. Substituting Eq. (2.61) into Eq. (2.60) and solving for ϵ_{12}^* yields:

$$\epsilon_{12}^* = (\bar{\mu} - \mu_f)\frac{\epsilon_{12}^\infty}{\bar{\mu} + 2\bar{S}_{1212}(\mu_f - \bar{\mu})} \tag{2.62}$$

Manipulating Eq. (2.62) to get the strain and stress field inside the particles gives the following two relations:

$$\epsilon_{12}^\infty + \epsilon_{12}^d = \bar{\mu}\frac{\epsilon_{12}^\infty}{\bar{\mu} + 2\bar{S}_{1212}(\mu_f - \bar{\mu})} \tag{2.63}$$

$$\sigma_{12}^\infty + \sigma_{12}^d = 2\mu_f\bar{\mu}\frac{\epsilon_{12}^\infty}{\bar{\mu} + 2\bar{S}_{1212}(\mu_f - \bar{\mu})} \tag{2.64}$$

The stress and strain fields inside the fibers are uniform, therefore, their average are equal to their uniform value. The relation between the average strain, $\langle\epsilon_{12}\rangle$, and stress, $\langle\sigma_{12}\rangle$, of the composite and its phases are as follows:

$$\langle\epsilon_{12}\rangle = \nu_M\langle\epsilon_{12}\rangle_M + \nu_f\langle\epsilon_{12}\rangle_f = \nu_M\langle\epsilon_{12}\rangle_M + \frac{\bar{\mu}}{\bar{\mu} + 2\bar{S}_{1212}(\mu_f - \bar{\mu})}\,\epsilon_{12}^\infty \tag{2.65}$$

$$\langle\sigma_{12}\rangle = \nu_M\langle\sigma_{12}\rangle_M + \nu_f\langle\sigma_{12}\rangle_f = \nu_M\langle\sigma_{12}\rangle_M + \frac{\mu_f\bar{\mu}}{\bar{\mu} + 2\bar{S}_{1212}(\mu_f - \bar{\mu})}\,2\epsilon_{12}^\infty \tag{2.66}$$

The quantities, $\langle\epsilon_{12}\rangle_M$ and $\langle\epsilon_{12}\rangle_f$, are the average strain in the matrix and particles, respectively and $\langle\sigma_{12}\rangle_M$ and $\langle\sigma_{12}\rangle_f$ are the average stress in the matrix and particles, respectively. Using Hooke's law in the matrix leads to

$$\langle\sigma_{12}\rangle_M = 2\,\mu_M\,\langle\epsilon_{12}\rangle_M \tag{2.67}$$

Based on the average theorem for infinitesimal strain in incompressible material under constant strain, ϵ_{ij}^{∞}, the average strain and stress over the whole composite material is equal to the applied stress and strain at the far-field, i,e.

$$\langle \sigma_{12} \rangle = \sigma_{12}^{\infty} \tag{2.68}$$

$$\langle \epsilon_{12} \rangle = \epsilon_{12}^{\infty} \tag{2.69}$$

Substituting Eqs. (2.67), (2.68) and (2.69) into Eqs. (2.65) and (2.66), and solving for $\langle \sigma_{12} \rangle$ as a function of $\langle \epsilon_{12} \rangle$ results in

$$\langle \sigma_{12} \rangle = \mu_M \langle 2\epsilon_{12} \rangle + \sum_{f=1}^{n} \nu_f (\mu_f - \mu_M) \frac{\bar{\mu}}{\bar{\mu} + 2\bar{S}_{1212}(\mu_f - \bar{\mu})} \langle 2\epsilon_{12} \rangle \tag{2.70}$$

and using the relation $\langle \sigma_{12} \rangle = \bar{\mu} \langle 2\epsilon_{12} \rangle$, it follows:

$$\bar{\mu} = \mu_M + \sum_{f=1}^{n} \frac{\nu_f (\mu_f - \mu_M)\bar{\mu}}{[\bar{\mu} + 2\bar{S}_{1212}(\mu_f - \mu_M)]} \tag{2.71}$$

Repeating the same procedure for σ_{11}, gives the effective bulk modulus as follows:

$$\bar{\kappa} = \kappa_M + \sum_{f=1}^{n} \frac{\nu_f (\kappa_f - \kappa_M)\bar{\kappa}}{[\bar{\kappa} + \frac{1}{3}\bar{S}_{iijj}(\kappa_f - \bar{\kappa})]} \tag{2.72}$$

The relations for the Eshelby tensor elements $\bar{S}_{iijj}$ and $\bar{S}_{1212}$ are as follows:

$$\bar{S}_{1212} = \frac{3(\bar{\kappa} + 2\bar{\mu})}{5(3\bar{\kappa} + 4\bar{\mu})} \tag{2.73}$$

$$\bar{S}_{iijj} = \frac{9\bar{\kappa}}{3\bar{\kappa} + 4\bar{\mu}} \tag{2.74}$$

Therefore, the above relations represent a set of nonlinear equations which may be solved simultaneously to find the values of $\bar{\mu}$, $\bar{\kappa}$ and $\bar{\nu}$ for given μ_f, κ_f and ν_f.

Homogeneously distributed spherical particles in an isotropic matrix yields an isotropic composite material. Therefore, the Eshelby tensor takes a simpler form than the

general form that was expressed in the previous section. The Eshelby tensor for a spherical particle in an isotropic material is as follows:

$$\bar{S}_{ijkl} = \frac{5\,\bar{\nu} - 1}{15(1-\bar{\nu})}\delta_{ij}\delta_{kl} + \frac{4 - 5\bar{\nu}}{15(1-\bar{\nu})}(\delta_{ik}\delta_{jl} + \delta_{jl}\delta_{jk}) \tag{2.75}$$

where $\bar{\nu}$, is the S-C approximation of the composite material Poisson ratio. Isotropic material properties in terms of Lamé's parameters λ and μ in indicial notation is expressed as follows:

$$\bar{C}_{ijkl} = \bar{\lambda}\delta_{ij}\delta_{kl} + \bar{\mu}(\delta_{ik}\delta_{jl} + \delta_{il}\delta_{jk}) \tag{2.76}$$

Considering isotropic material properties for the matrix and inhomogeneity and also spherical particles, the eigenstrain is evaluated using the expression derived in the previous section which is printed below as well:.

$$C^{f}_{ijkl}(\epsilon^{\infty}_{kl} + \bar{S}_{klmn}\,\epsilon^{*}_{mn}) = \bar{C}_{ijkl}(\epsilon^{\infty}_{kl} + \bar{S}_{klmn}\,\epsilon^{*}_{mn} - \epsilon^{*}_{kl}) \tag{2.77}$$

Substituting the S-C approximation of the composite material properties and the Eshelby tensor derived from the effective properties into Eq. (2.77) leads to the following concise expression for eigenstrain ϵ^{*}_{ij}.

$$A = (3\bar{\kappa} + 4\bar{\mu})15\bar{\kappa}(3\kappa_f + 4\bar{\mu})(\bar{\mu} - \mu_f)\epsilon^{\infty}_{ij} \tag{2.78}$$

$$B = (3\bar{\kappa} + 4\bar{\mu})\big(-4\bar{\kappa}\bar{\mu}(2\bar{\mu} + 3\mu_f) + \bar{\kappa}^2(9\bar{\mu} + 6\mu_f) + \bar{\kappa}(-24\kappa_f\bar{\mu} - 12\bar{\mu}^2 + 9\kappa_f\mu_f + 32\bar{\mu}\mu_f)\big) \tag{2.79}$$

$$\epsilon^{*}_{ij} = \frac{A\,\epsilon^{\infty}_{ij} + B\,\delta_{ij}\epsilon^{\infty}_{nn}}{3\bar{\kappa}(3\kappa_f + 4\bar{\mu})(9\bar{\kappa}\bar{\mu} + 8\bar{\mu}^2 + 6\bar{\kappa}\mu_f + 12\bar{\mu}\mu_f)} \tag{2.80}$$

where the quantities ,$\bar{\kappa}$ and $\bar{\mu}$, are the S-C approximation of the bulk modulus and shear modulus of the composite material, respectively. Also the quantities, κ_f and μ_f, are the bulk modulus and shear modulus of the particles, respectively. The repeated indices are to be summed over. The above expressions show that the eigenstrain is uniform inside

the inhomogeneity. The strain and stress inside the particle are expressed in terms of the eigenstrain as:

$$\epsilon_{kl}^{in} = \epsilon_{kl}^{\infty} + \bar{S}_{klmn}\,\epsilon_{mn}^{*} \tag{2.81}$$

$$\sigma_{ij}^{in} = C_{ijkl}^{f}(\epsilon_{kl}^{\infty} + \bar{S}_{klmn}\,\epsilon_{mn}^{*}) \tag{2.82}$$

Substituting Eqs. (2.75) and (2.76) into Eqs. (2.81) and (2.82) gives the explicit form of the stress and strain inside the spherical particles as

$$\epsilon_{kl}^{in} = \frac{(3\bar{\kappa}+4\bar{\mu})\big(5\bar{\mu}(3\kappa_f+4\bar{\mu})\epsilon_{kl}^{\infty} + \big(\bar{\kappa}(3\bar{\mu}+2\mu_f)+\bar{\mu}(-5\bar{\kappa}-4\bar{\mu}+4\mu_f)\big)\delta_{kl}\epsilon_{nn}^{\infty}\big)}{(3\kappa_f+4\bar{\mu})(9\bar{\kappa}\bar{\mu}+8\bar{\mu}^2+6\bar{\kappa}\mu_f+12\bar{\mu}\mu_f)} \tag{2.83}$$

$$\sigma_{ij}^{in} \tag{2.84}$$

$$= \frac{(3\bar{\kappa}+4\bar{\mu})\big(30\bar{\mu}(3\kappa_f+4\bar{\mu})\mu_f\epsilon_{ij}^{\infty}\big)}{3(3\kappa_f+4\bar{\mu})(9\bar{\kappa}\bar{\mu}+8\bar{\mu}^2+6\bar{\kappa}\mu_f+12\bar{\mu}\mu_f)}$$

$$+\frac{(3\bar{\kappa}+4\bar{\mu})\Big(9\bar{\kappa}\kappa_f(3\bar{\mu}+2\mu_f)+2\bar{\mu}\big(-20\bar{\mu}\mu_f+3\kappa_f(4\bar{\mu}+\mu_f)\big)\Big)\delta_{ij}\epsilon_{nn}^{\infty}}{3(3\kappa_f+4\bar{\mu})(9\bar{\kappa}\bar{\mu}+8\bar{\mu}^2+6\bar{\kappa}\mu_f+12\bar{\mu}\mu_f)}$$

To calculate the stress outside the particles based on the stress inside the particles, we evaluate the jump parameter through solving Eq. (2.56) which is printed bellow:

$$\bar{C}_{ijkl}\lambda_k\,n_l\,n_i = -\sigma_{ij}^{*}n_i \tag{2.85}$$

Using the explicit expression for isotropic material properties and eigenstrain, Eq. (2.80), in Eq. (2.85) and solving the resulted set of linear equations gives the jump parameter as follows:

$$A = 10(3\bar{\kappa}+\bar{\mu})(3\kappa_f+4\bar{\mu})(\bar{\mu}-\mu_f) \tag{2.85}$$

$$B = -10(3\bar{\kappa}+4\bar{\mu})(3\kappa_f+4\bar{\mu})(\bar{\mu}-\mu_f) \tag{2.86}$$

$$C = -27\bar{\kappa}^2\bar{\mu} + 27\bar{\kappa}\kappa_f\bar{\mu} - 24\bar{\kappa}\bar{\mu}^2 + 54\kappa_f\bar{\mu}^2 + 40\bar{\mu}^3 - 18\bar{\kappa}^2\mu_f + 18\bar{\kappa}\kappa_f\mu_f \tag{2.87}$$

$$- 36\bar{\kappa}\bar{\mu}\mu_f + 6\kappa_f\bar{\mu}\mu_f - 40\bar{\mu}^2\mu_f$$

$$D = (3\kappa_f + 4\bar{\mu})\big(\bar{\mu}(9\bar{\kappa} + 8\bar{\mu}) + 6(\bar{\kappa} + 2\bar{\mu})\mu_f\big) \tag{2.88}$$

$$\lambda_j = \frac{A\, n_j n_m n_l \epsilon^{\infty}_{lm} + B\, n_m \epsilon^{\infty}_{jm} + C\, n_j \epsilon^{\infty}_{mm}}{D} \tag{2.89}$$

where repeating indices are to be summed over. The quantities, $\bar{\kappa}$ and $\bar{\mu}$, are the effective bulk and shear modulus of the composite material which were expressed in Eqs. (2.71) and (2.72). The quantities, κ_f and μ_f, are the bulk and shear modulus of the particles, respectively. Having solved for the jump parameter, the stress field outside the particles is evaluated using Eq. (2.58) which is printed bellow as well:

$$\sigma^{out}_{ij} = \bar{C}_{ijkl}(\epsilon^{\infty}_{kl} + \bar{S}_{klmn}\, \epsilon^{*}_{mn}) - \bar{C}_{ijkl}\lambda_k\, n_l \tag{2.90}$$

Substituting the isotropic material property relation, Eq. (2.76), and the relation for λ_i , Eq. (2.89), into Eq. (2.90) gives the following explicit relation for stress outside the particle σ^{out}_{or} as:

$$A = 30\bar{\mu}(3\kappa_f + 4\bar{\mu})(\bar{\mu} - \mu_f) \tag{2.91}$$

$$B = 270\bar{\kappa}\kappa\bar{\mu}^2 + 360\bar{\kappa}\bar{\mu}^3 + 360\kappa_f\bar{\mu}^3 + 480\bar{\mu}^4 \tag{2.92}$$

$$\begin{aligned} C = {} & -162\bar{\kappa}^2\bar{\mu}^2 + 162\bar{\kappa}\kappa_f\bar{\mu}^2 - 144\bar{\kappa}\bar{\mu}^3 + 324\kappa_f\bar{\mu}^3 + 240\bar{\mu}^4 - 108\bar{\kappa}^2\bar{\mu}\mu_f \\ & + 108\bar{\kappa}\kappa_f\bar{\mu}\mu_f - 216\bar{\kappa}\bar{\mu}^2\mu_f + 36\kappa_f\bar{\mu}^2\mu_f - 240\bar{\mu}^3\mu_f \end{aligned} \tag{2.93}$$

$$\begin{aligned} D = {} & 81\bar{\kappa}^2\kappa_f\bar{\mu} + 162\bar{\kappa}^2\bar{\mu}^2 + 18\bar{\kappa}\kappa_f\bar{\mu}^2 + 144\bar{\kappa}\bar{\mu}^3 - 228\kappa_f\bar{\mu}^3 - 240\bar{\mu}^4 \\ & + 54\bar{\kappa}^2\kappa_f\mu_f + 108\bar{\kappa}^2\bar{\mu}\mu_f - 18\kappa\epsilon\kappa_f\bar{\mu}\mu_f + 96\bar{\kappa}\bar{\mu}^2\mu_f \\ & - 12\kappa_f\bar{\mu}^2\mu_f + 80\bar{\mu}^3\mu_f \end{aligned} \tag{2.94}$$

$$\begin{aligned} E = {} & 81\bar{\kappa}\kappa_f\bar{\mu} + 108\bar{\kappa}\bar{\mu}^2 + 72\kappa_f\bar{\mu}^2 + 96\bar{\mu}^3 + 54\bar{\kappa}\kappa_f\mu_f + 72\bar{\kappa}\bar{\mu}\mu_f + 108\kappa_f\bar{\mu}\mu_f \\ & + 144\bar{\mu}^2\mu_f \end{aligned} \tag{2.95}$$

$$\sigma_{or}^{out} = \frac{A\left(2n_j n_k n_o n_r \epsilon_{jk}^{\infty}(3\bar{\kappa}+\bar{\mu}) + n_j n_k \delta_{ro}\epsilon_{jk}^{\infty}(-3\bar{\kappa}+2\bar{\mu})\right)}{E} \quad (96)$$

$$- \frac{A(n_j n_r \epsilon_{jo}^{\infty} + n_j n_o \epsilon_{jr}^{\infty})(3\bar{\kappa}+4\bar{\mu})}{E}$$

$$+ \frac{+B\epsilon_{or}^{\infty} + (\mathrm{C}n_o n_r + \mathrm{D}\delta_{ro})\epsilon_{jj}^{\infty}}{E}$$

This relation provides the stress field on the interface, inside the matrix in terms of the applied strain at the far-field, the effective properties of the composite material and the properties of the particles. In case the applied far-field loading is in stress form, the strain relation at the far-field is expressed in terms of the applied stress explicitly as follows:

$$\epsilon_{ij}^{\infty} = \frac{9\bar{\kappa}\sigma_{ij}^{\infty} + (-3\bar{\kappa}+2\bar{\mu})\delta_{ij}\sigma_{nn}^{\infty}}{18\bar{\kappa}\bar{\mu}} \quad (2.97)$$

2.4 Failure criterion

In the foregoing, the stress fields inside and outside a particle were determined in terms of the applied far-field loading, the particle geometry and the S-C approximation of the composite material properties. To determine the maximum allowable far-field loading, the obtained local stresses are substituted into the von Mises failure criterion. This provides the necessary formula to obtain the failure envelopes of the composite materials in various loading scenarios.

The stresses at the interface are now formulated in terms of the matrix properties, the reinforcing element properties and reinforcement volume fraction as well as the applied loading. We substitute the interface stresses in a failure criterion and evaluate the maximum allowable applied far-field loading. The von Mises failure criterion will be used because it embeds the quadratic form and coupling characteristics of composite failure criterion. The von Mises relation is as follows:

$$\sigma_{vMises} = \sqrt{\frac{3}{2}\sigma'_{ij}\sigma'_{ij}} \tag{2.98}$$

where σ'_{ij} is the deviatoric part of the stress. Substituting the deviatoric stress relations outside the particles into Eq. (2.98) gives the von Mises stress field on the surface of the particles in terms of the applied loading at the far-field .

Equation (2.98) gives the von Mises stress field on the interface and is to be maximized. The resulting expression is very complex and could not be expressed analytically for the locus of maximum. The location where the maximum von Mises stress happens is a function of the applied loading, therefore, we evaluated the maximum location for various loading scenarios separately. Each point on a 2-D failure envelope graph corresponds to a loading scenario that consist of loading in the first direction σ_1^∞, and the ratio between the loading in the second direction to the loading in the first direction, $\rho = \sigma_2^\infty/\sigma_1^\infty$. We first divide the space into 200 points which consist of 200 pairs of ratio, ρ, and loading in first direction, σ_1^∞. The ratio, ρ, ranges from -1 to 1. We set σ_1^∞ equal to 1 and solve the resulting expression for the magnitude of the maximum von Mises stress numerically. Then based on the maximum value and yielding strength, we scale the loading in first direction to get the allowable loading at the far-field.

2.5 Results

This chapter presents the results from the previously developed relations between the applied far-filed mechanical loading and allowable local stresses for the matrix material. The material properties used in the following results are chosen from Tables (2-1) and (2-2). The isotropic material properties are for the isotropic results and the transversely isotropic material properties are for the transversely isotropic results

wherever applicable. In the special cases of rigid particles and cavity, only the matrix properties are applicable.

Table 2-1 Isotropic fiber and matrix properties

Isotropic material	E (GPa)	ν
Fiber	140	0.33
Matrix	70	0.33

Table 2-2 Transversely isotropic fiber and matrix properties

Transversely isotropic material	E_1	E_3	ν_{12}	ν_{13}	G_{13}
Fiber	26	130	0.3	0.3	10
Matrix	2.6	5.2	0.3	0.3	1

The results from the Eshelby approach are compared to the results from a series solution in Figs. (2-1) and (2-2). The graphs show very good agreement between these two approaches. The examples considered are two extreme cases of cavity and rigid particles inside an unbounded matrix phase, while the matrix is transversely isotropic.

Figure (2-1) depicts the stress in the "*z"* direction along the equator of a cavity embedded in a transversely isotropic matrix where the stress concentration is the highest. The results from current study are compared to the results from Kusch [21]. Kusch used a series solution to the inhomogeneity problem. As expected, these results are in close agreement. The results are drawn for two different anisotropy parameter (E_3/E_1) values, 1 and 10. The graphs show that the anisotropy parameter affects the

stress concentration significantly. Increasing this parameter causes higher stress concentration values around the particles.

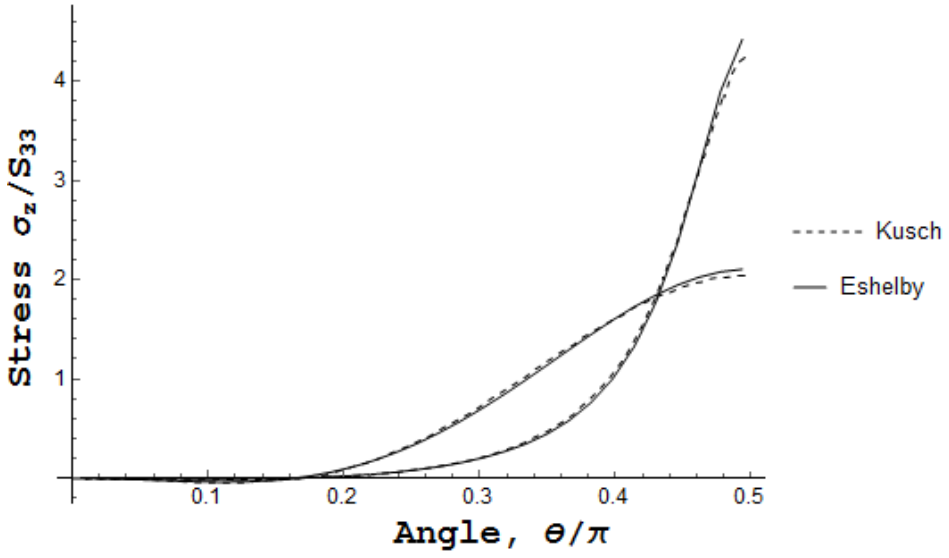

Figure 2-1 Stress σ_z along a cavity surface.

Figure (2-2), presents the stress field on the equator of a rigid particle embedded in a transversely isotropic matrix. These graphs are for two different matrix anisotropy parameter, 1 and 10. The results are in very close agreement with the results from the series solution conducted by Kusch [21]. The stress concentration for an isotropic matrix (anisotropy parameter equal 1) is 1.3. Increasing the anisotropy parameter, raises the stress concentration value significantly.

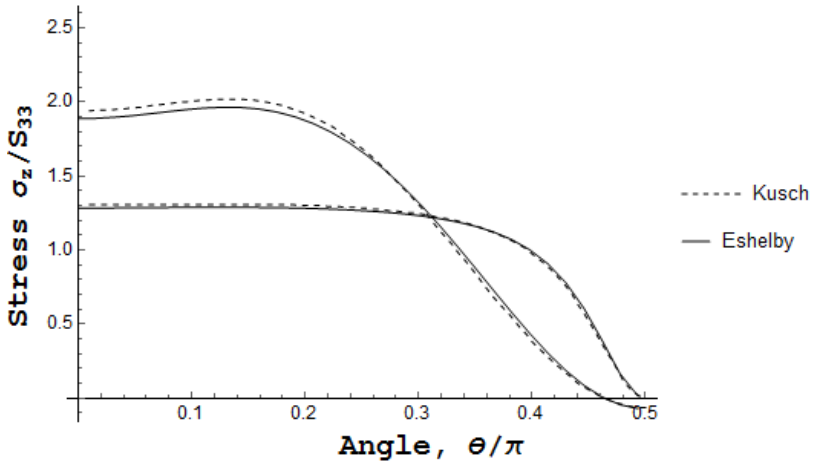

Figure 2-2 Stress σ_z along the matrix- particle interface.

2.5.1 Cavity

The particle aspect ratio is one of the parameters that is relatively under manufacturing control. Since we are studying the spheroid shaped voids, we define the aspect ratio, ρ, as the ratio of diameter in the first direction to the diameter in the third direction. i.e, ρ larger, equal and smaller than unit denote oblate, sphere and prolate, respectively. This parameter affects the stress concentration significantly. Before proceeding to discuss the results in Figs. (2-3) to (2-5) on an individual basis, it is worthwhile to mention that as a general rule if the applied loading is in the third direction, increasing the ratio leads to higher values of stress concentration around the void.

Figures (2-3) and (2-4) present the von Mises stress concentration around a spheroid cavity with varying aspect ratios of the cavity. A high aspect ratio makes a penny shaped cavity and smaller than 1 aspect ratio simulates a slender needle shaped cavity. Pulling a needle shaped cavity does not make much stress concentration but pulling on a penny shaped cavity has very large stress concentrations around the edges. Figure (2-3) illustrates the von Mises stress concentration around oblate spheroids under loading in the third direction. The stress concentration is approximately a linear function

of the ratio of the oblate spheroid. As a rule of thumb, in this case the von Mises stress concentration is twice the aspect ratio of the oblate spheroid.

The von Mises stress concentration for the prolate cavity under loading in the third direction is illustrated in Fig. (2-4) as a function of the aspect ratio, ρ. The von Mises stress concentration is equal to 3 for the sphere. This value decreases with decreasing the prolate aspect ratio.

The von Mises stress concentration around three cavities with aspect ratios equal to 0.2, 1 and 5 is illustrated in Fig. (2-5). Since the stresses in these cases have a radial symmetry property, only a portion of the stress is shown. The location of the stress concentration for all of the cavities is on the equator and the lowest stress is located close to the poles of the cavities.

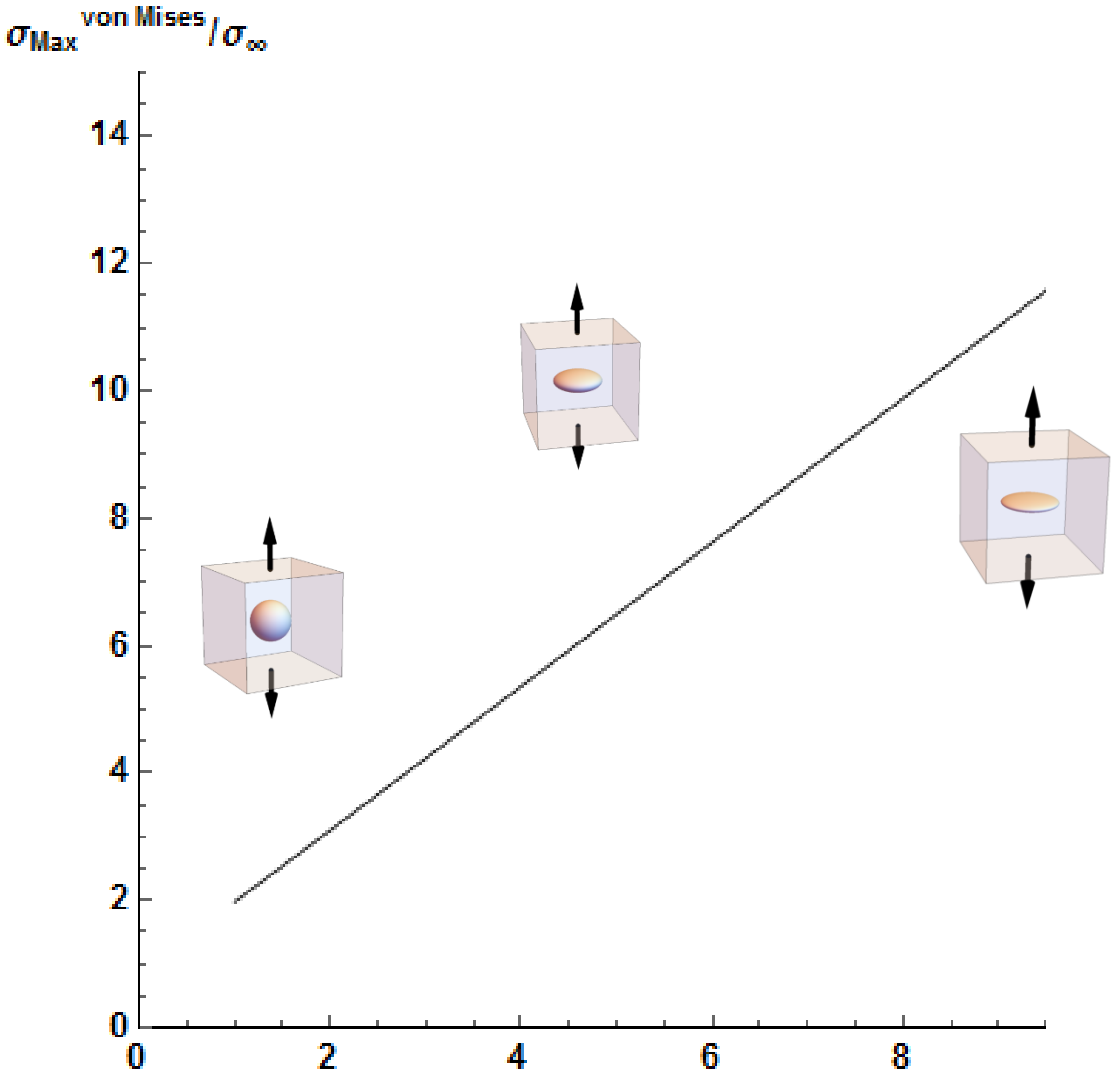

Figure 2-3 Effect of oblate shaped cavity aspect ratio on the maximum von Mises stress under σ_∞^z.

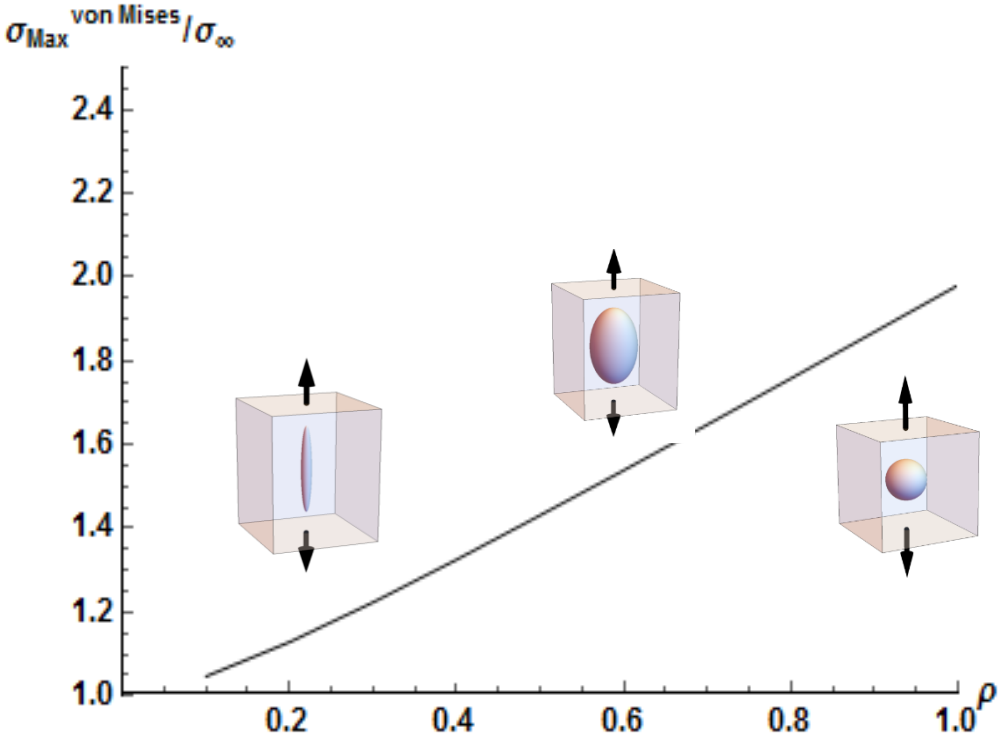

Figure 2-4 Effect of prolate shaped cavity aspect ratio on the maximum von Mises stress under σ_∞^z.

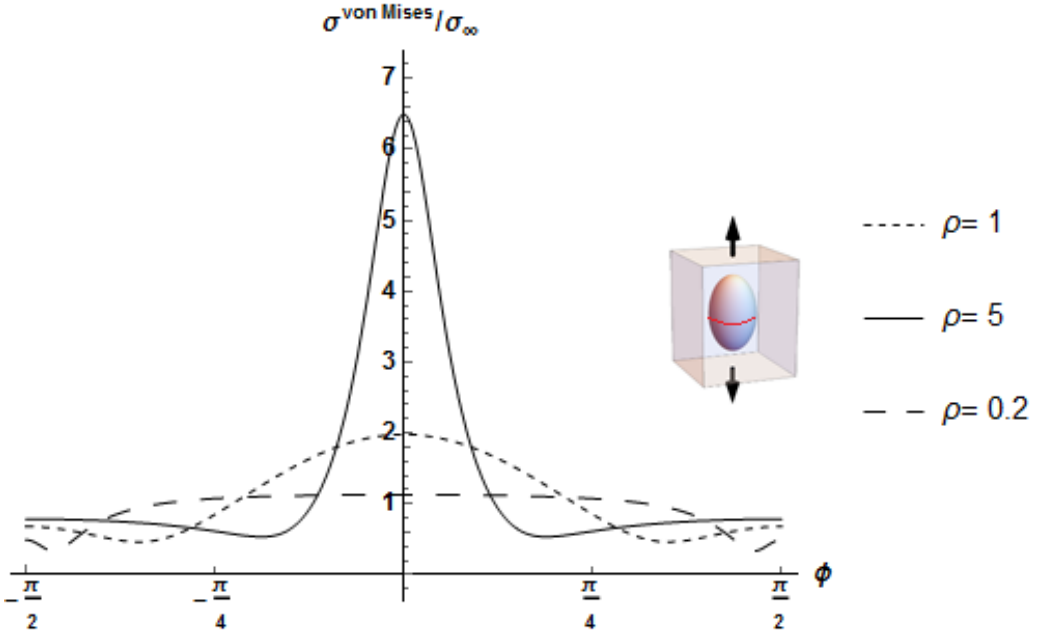

Figure 2-5 The von Mises stress distribution along the equator of a cavity under σ_∞^z.

2.5.2 Rigid particle

In the forgoing results, the von Mises stress concentration around a cavity embedded in a matrix material was illustrated and discussed. Here we discuss the von Mises stress concentration around a rigid particle which is the opposite extreme case of a cavity. The results are interesting and are worth investigation.

Figure (2-6) shows a non-monotonic behavior of the von Mises stress concentration as a function of the rigid particle aspect ratio under loading in the third direction. According to this graph, increasing the aspect ratio of the rigid particle from 1 to 20 first causes reduction in the stress concentration with the minimum value at around ρ equal to 5. After this minimum value, increasing the ratio of the particle shape increases the von Mises stress concentration. The figures in this section are for very stiff particles,

but in later sections the stress concentration for varying stiffness of the particles will be studied. When the particles have prolate shape, i.e. their aspect ratio is less than 1, the behavior is different from the case where we had cavities of the same shape. The von Mises stress concentration in case of rigid particles is much higher than the case for cavities. Also decreasing the aspect ratio has an inverse effect on the von Mises stress concentration. In this graph, the matrix Poisson ratio is equal to 0.3. The Poisson ratio affects the value of the von Mises stress concentration but does not change the overall graph's behavior.

Figure (2-8) shows the distribution of the von Mises stress on the particle's meridian line which is located at $\theta = const$. Angles $\emptyset = -\pi/2$ and $\emptyset = \pi/2$ correspond to the poles of the particles. According to this graph, the maximum von Mises stress is located at $\emptyset = \pi/4$, halfway between the poles and equator. The maximum von Mises stress value is located around the equator for oblate particles and close to the poles around prolate particles. Also these graphs are in agreement with the previous interpretation stating that prolate rigid particles cause more stress concentration than oblate rigid particles.

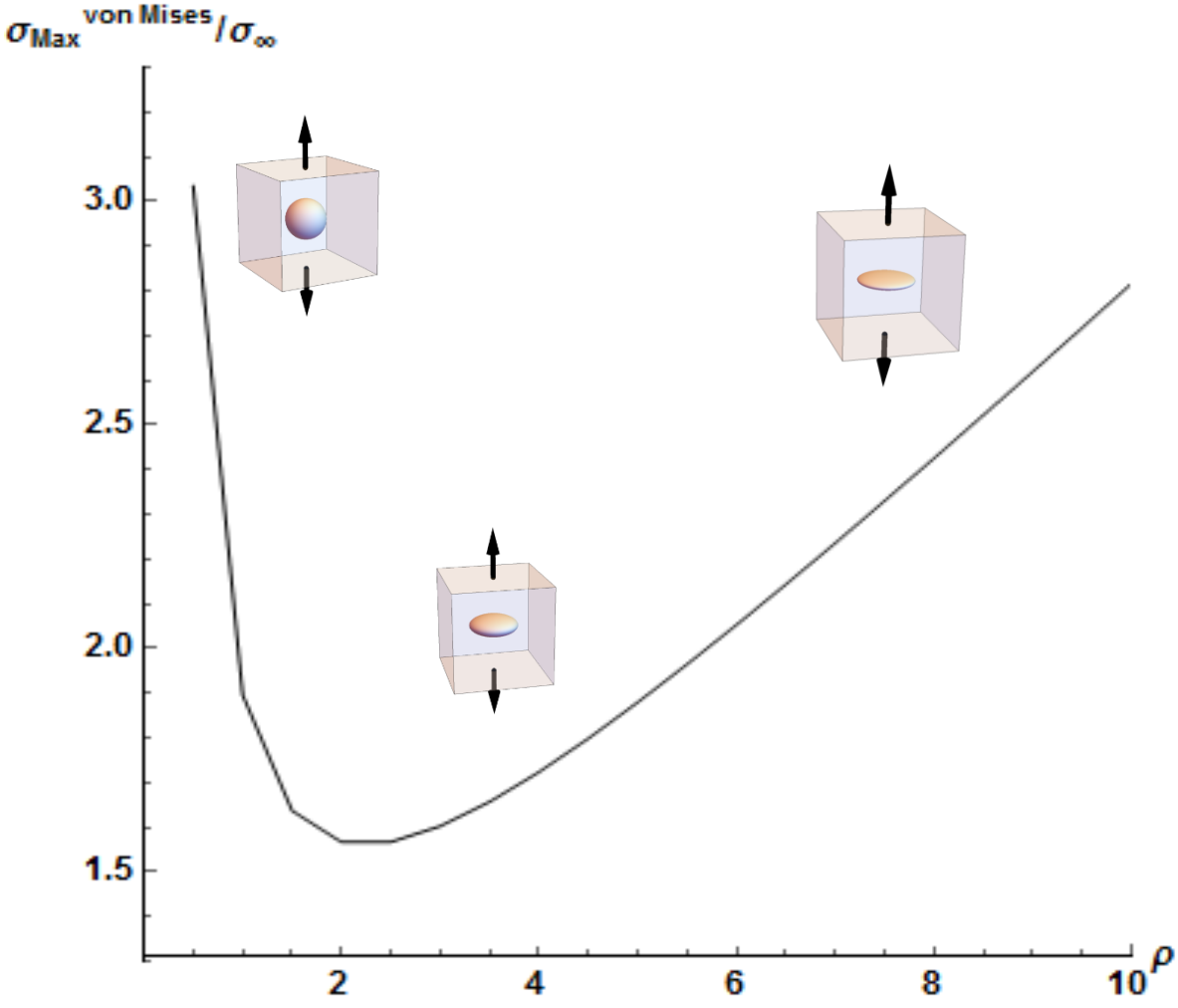

Figure 2-6 The maximum von Mises stress around oblate shaped rigid particles inside an unbounded isotropic material under σ_{∞}^{z}.

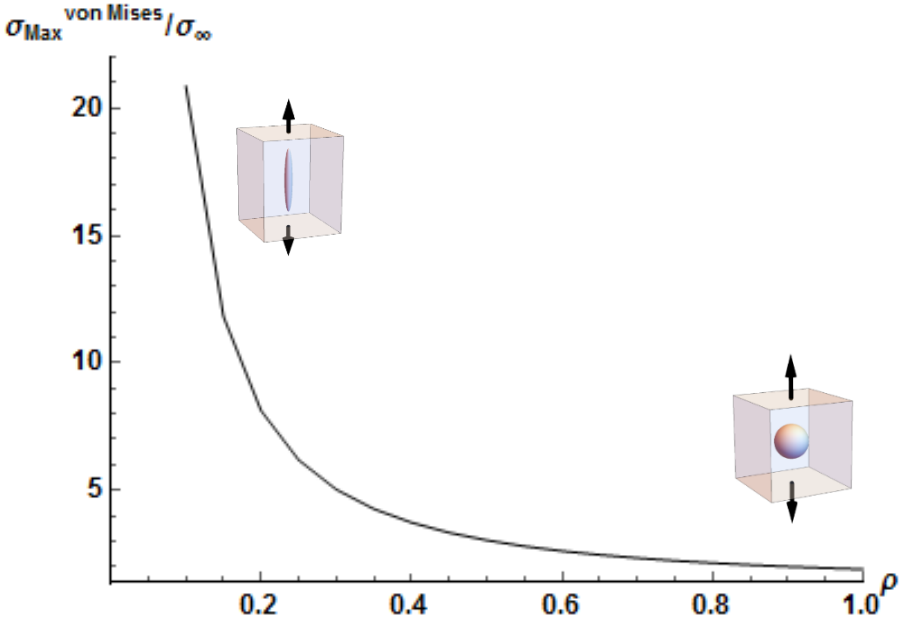

Figure 2-7 The maximum von Mises stress around prolate shaped rigid particles inside an unbounded isotropic material under σ_∞^z.

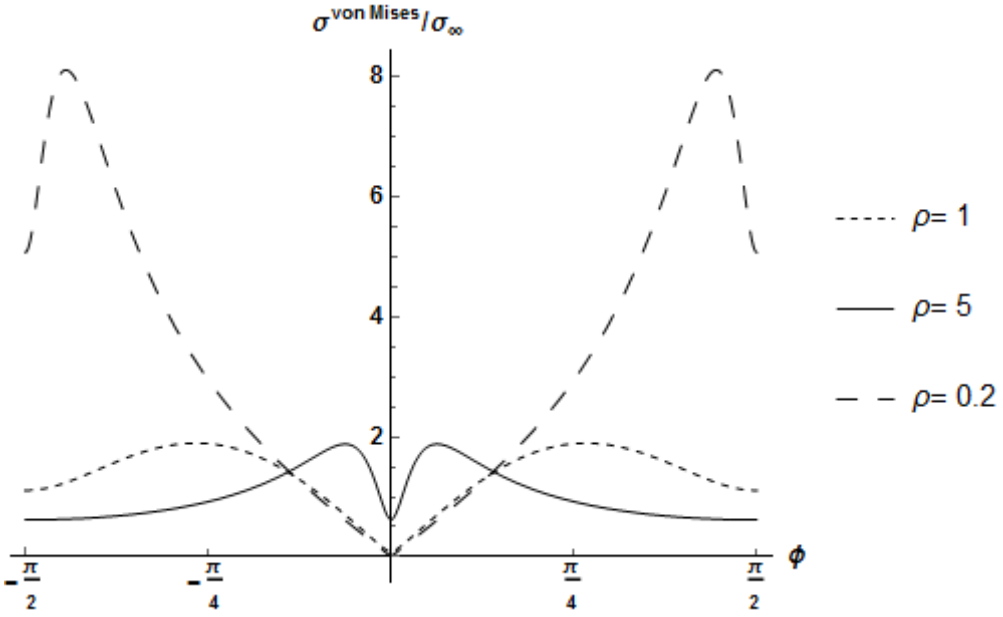

Figure 2-8 The von Mises stress distribution along the equator of a sphere, oblate and prolate shaped rigid particle in an unbounded isotropic matrix material under σ_∞^z.

2.5.3 Elastic particle

In the foregoing results, the effect of aspect ratio on the stress distribution around a cavity and rigid particle as the two extreme cases of particles was investigated. Here the effect of particle stiffness on the von Mises stress concentration is studied. To study this effect, we plot a graph of the maximum von Mises stress around a prolate, oblate and spherical particle with respect to varying particle to matrix stiffness ratios. As expected at the stiffness ratio equal to 1, there is no stress concentration around the particles because this simulates the homogeneous isotropic material. Increasing the particle to matrix stiffness ratio raises the stress concentration of all three kinds of particles. This parameter has the maximum effect on the prolate spheroidal particles for particles stiffer than the matrix. If the matrix is stiffer than the particles, which happens in case of impurities, oblate spheroidal particles are affected by the stiffness ratio most.

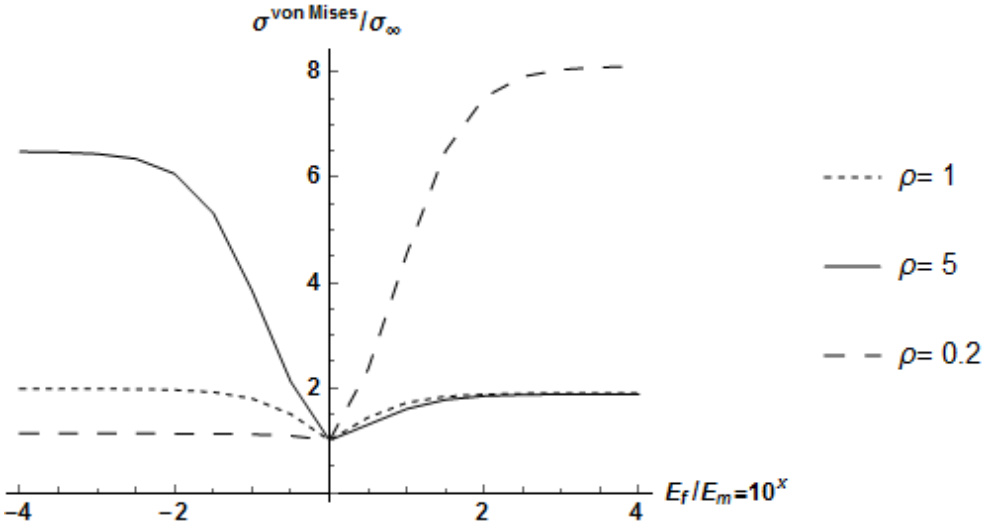

Figure 2-9 Effect of particle to matrix stiffness, $\frac{E_f}{E_m}$, on the maximum von Mises stress in sphere, oblate and prolate shaped particles in an unbounded transversely isotropic material under σ_∞^z.

The stresses outside the particles were evaluated and analyzed in the previous sections. It is worthwhile to study the stresses inside the particles and compare them to the stresses outside the particles. Figures (2-11) and (2-14) depict the von Mises stress inside the particles and the maximum von Mises stress outside the particles as a function of the particle aspect ratio. The stress inside the particles is uniform but the stress outside the particles is a function of the location. The stress values are normalized with respect to the applied far-field stress. As expected under normal stress at the far-field, Figs. (2-11) and (2-12), the particles are the load bearing elements, therefore, the von Mises stresses inside the particles are higher than the maximum von Mises stress inside the matrix. The minimum value of the stress concentration is located around an oblate particle with aspect ratio approximately equal to 2.

The other influencing factor to consider is the type of loading applied on the composite materials. In the previous results, the applied far-field loading was normal stress. Here we examine the effect of the applied shear stress at the far-field. According to Figs. (2-13) and (2-14), the stress concentration has a monotonically increasing behavior with varying particle aspect ratios. Around oblate particles, the stress concentration due to applied shear loading is larger than the stress concentration due to applied normal loading. Around prolate particles, the stress concentration under applied shear loading is smaller than under normal loading. Figure (2-13) shows that under in-plane shear loading the maximum von Mises stress on the interface is equal to the uniform von Mises stress inside the particle.

Here a comparison between the stresses inside and outside the particle under various loading condition is carried out. Figures (2-11) and (2-12) show that under applied normal stress at the far-field, the stresses inside the particles are greater than the stresses outside the particle. But the difference is lower than the difference between the particles and matrix strength. Therefore, the first yielding is still expected to happen inside the matrix rather than the particles. This trend is valid for various particle aspect ratios. These graphs show the differences between the normalized von Mises stresses inside and outside the particles for particle aspect ratios from 0.1 to 10. Figures (2-13) and (2-14) show that the von Mises stress under shear loading inside and outside the particles are equal. These graphs have a monotonic behavior and increasing the particle aspect ratio, monotonically increases the maximum von Mises stress inside and outside the particles.

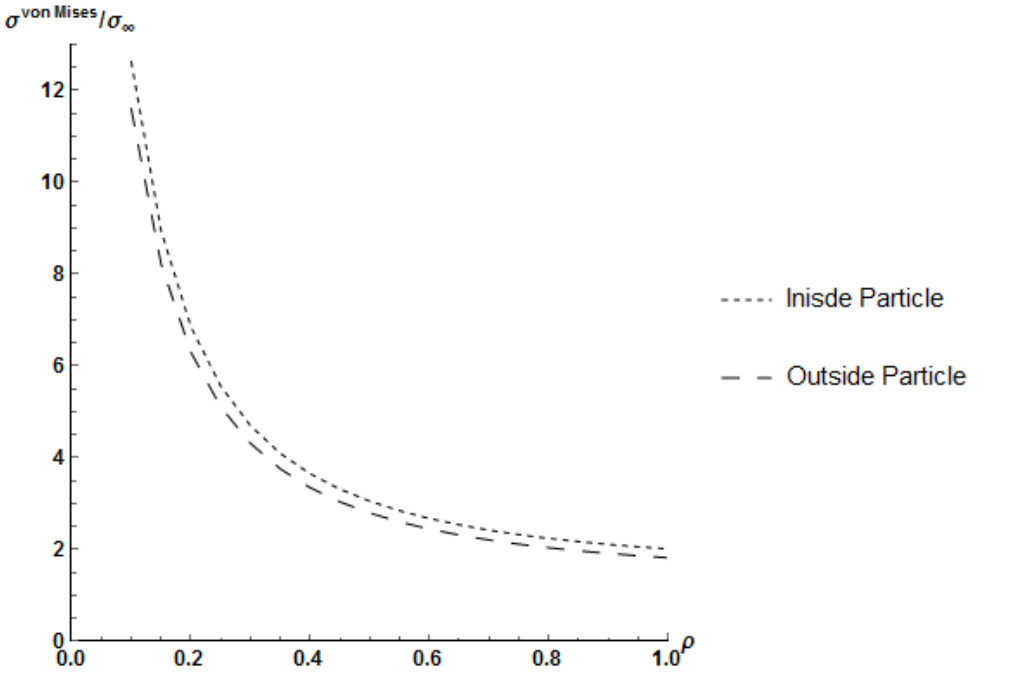

Figure 2-10 Comparison between stress inside and outside the particles in prolate shaped isotropic particles under normal stress, σ_∞^z.

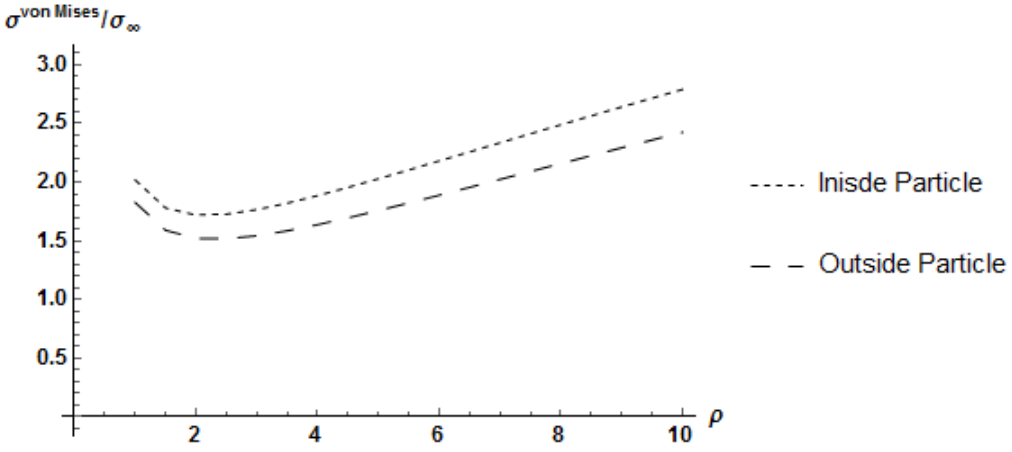

Figure 2-11 Comparison between stress inside and outside the particles in oblate shaped isotropic particles under normal stress, σ_∞^z.

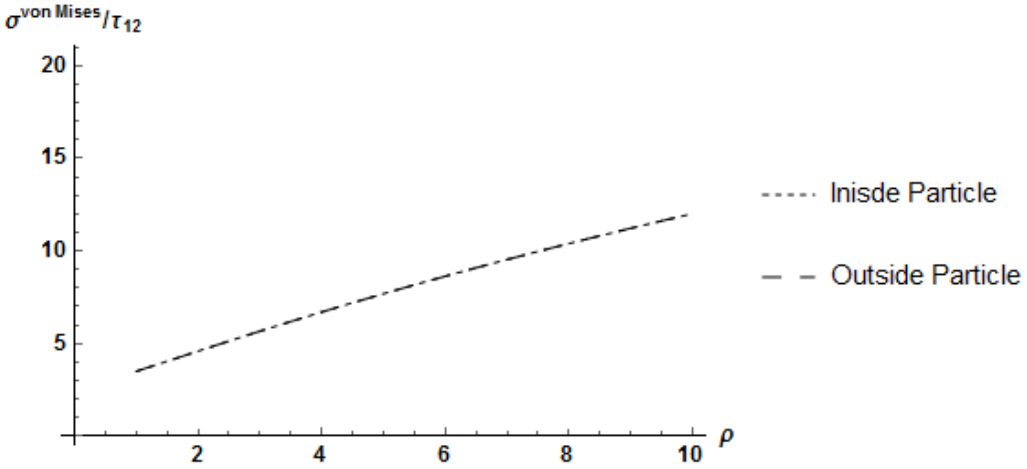

Figure 2-12 Comparison between stress inside and outside the particles in oblate shaped isotropic particles under shear stress, τ_{∞}^{z}.

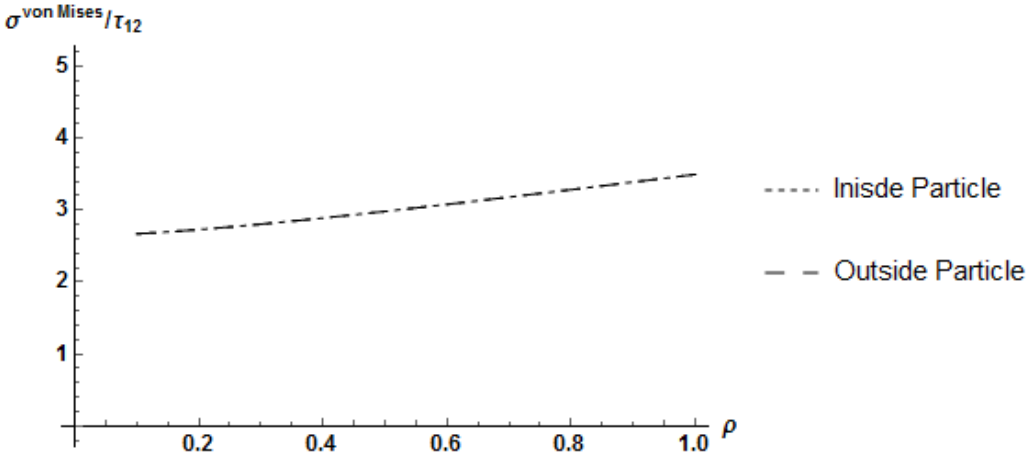

Figure 2-13 Comparison between stress inside and outside the particles in prolate shaped isotropic particles under shear stress, τ_{∞}^{z}.

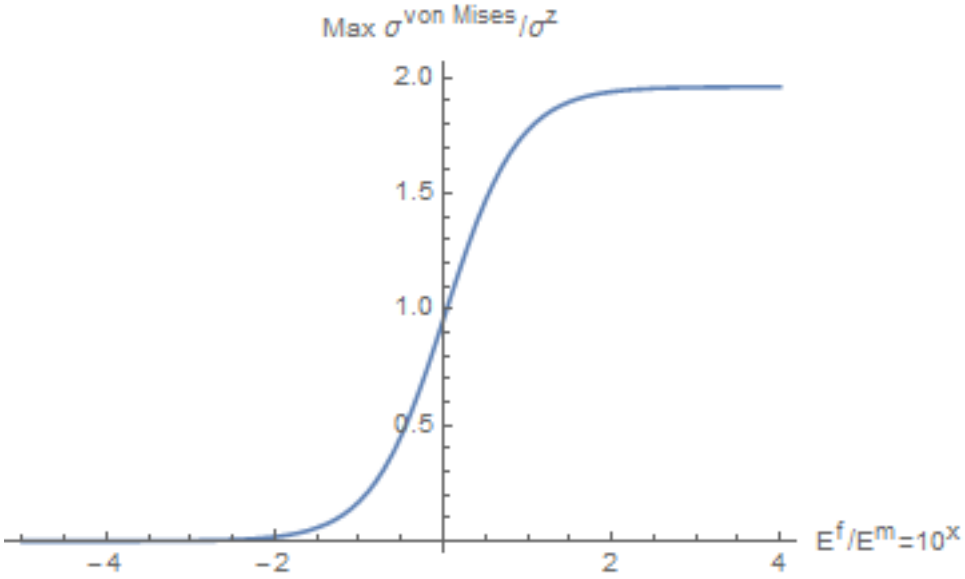

Figure 2-14 Effect of particle to matrix stiffness ratio on the maximum von Mises stress around a spherical particle in an unbounded isotropic matrix material under normal stress, σ_{∞}^{z}.

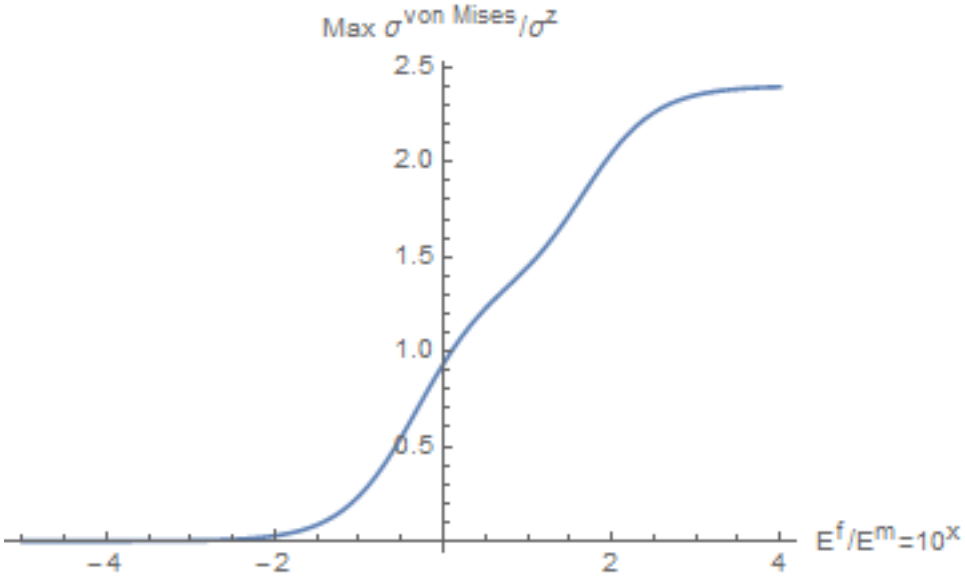

Figure 2-15 Effect of particle to matrix stiffness ratio on the von Mises stress around a prolate shaped particle in an unbounded isotropic matrix material under normal stress, σ_{∞}^{z}.

2.5.4 Failure envelope

The foregoing results were to investigate the effect of various parameters on the stress fields inside and outside the particles and the stress concentration. Here we try to put all the information into practice and examine the failure envelope for the composite materials as a function of the varying parameters such as the loading scenario, the particle to matrix stiffness ratio, the particles aspect ratio and also the volume fraction of the particles.

The particle volume fraction is one of the variables that could be tailored to the specific needs of the application. This parameter affects the stress distribution and overall behavior of the composite materials. Increasing the particle volume fraction generally increases the stiffness of the material and lowers the stress concentrations around the

particles. There are various forms of failure type among which matrix yielding is under study in this research. The matrix yielding is due to the stress concentration around the particles, therefore, increasing the particle volume fraction is expected to strengthen the composite materials against the matrix yielding failure. To investigate these qualitative expectation quantitatively, failure envelopes as a function of the particle volume fraction for various types of particle shape is examined below. Figures (2-17) to (2-26) show the failure envelopes for various particle shapes as a function of the particle volume fraction. The applied stress is normalized with respect to yielding strength of pure matrix, σ_M^y.

2.5.4.1 Isotropic matrix and particles

Figure (2-17) depicts the failure envelope for composites containing spherical particles for three values of particle volume fraction, 5%, 20% and 40%. As expected, increasing the particle volume fraction expands the failure envelopes, i.e., increases the strength of the composite materials. It is obvious that the yielding strength of the composite material is less than the yielding strength of the matrix material. This is due to the stress concentration around the particles. The inserted particles decrease the yielding strength of the material but matrix yielding is not the ultimate strength of the composite material. In later steps of the failure, these particles obstruct the progress of the cracks and also they decrease the overall stress distribution inside the matrix which slows down the crack developments.

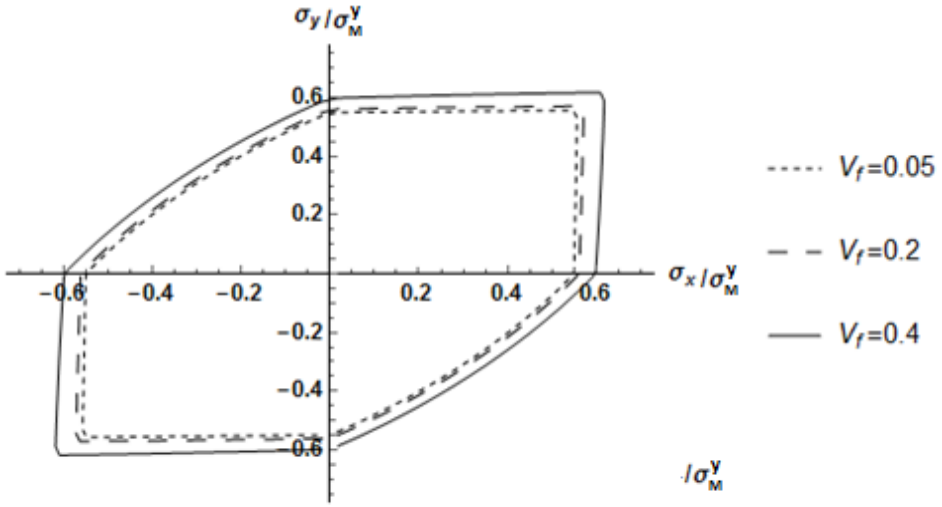

Figure 2-16 Failure envelope for a particulate reinforced composite embedding spherical reinforcing particles under loading in x-y plane.

In the following graphs, the effect of changing particle aspect ratio on the failure envelopes is examined. Figure (2-18) includes three plots for the particle volume fractions 5%, 20% and 40%. All three graphs show that increasing the volume fraction, expands the failure envelopes for various loading scenarios except for a segment corresponding to normal tension-normal compression case in which increasing the volume fraction does not affect the failure envelopes significantly.

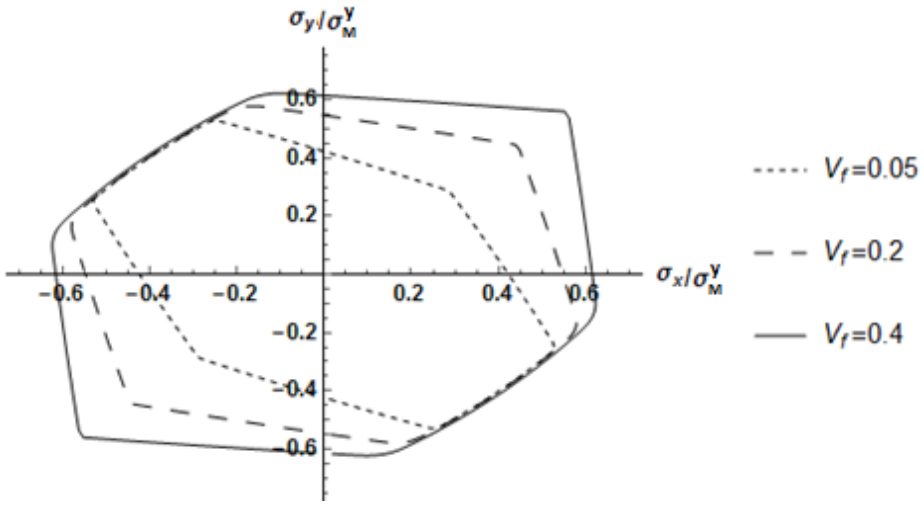

Figure 2-17 Failure envelope for a particlulate reinforced composite embedding prolate ($\rho = 0.1$) reinforcing particles under loading in the x-y plane.

In order to compare the effect of particle aspect ratio on the failure envelopes, the graphs are put in one plot in Fig. (2-20). The particle aspect ratios 1, 0.1 and 0.01 and isotropic matrix material are considered. The graphs are for the volume fraction equal to 20%. This graph shows that decreasing the particle aspect ratio strengthens the composite material in a tension-compression loading scenario but decreases the strength in a tension-tension loading scenario, i.e., prolate particles make less stress concentration in tension-compression than tension-tension loading condition.

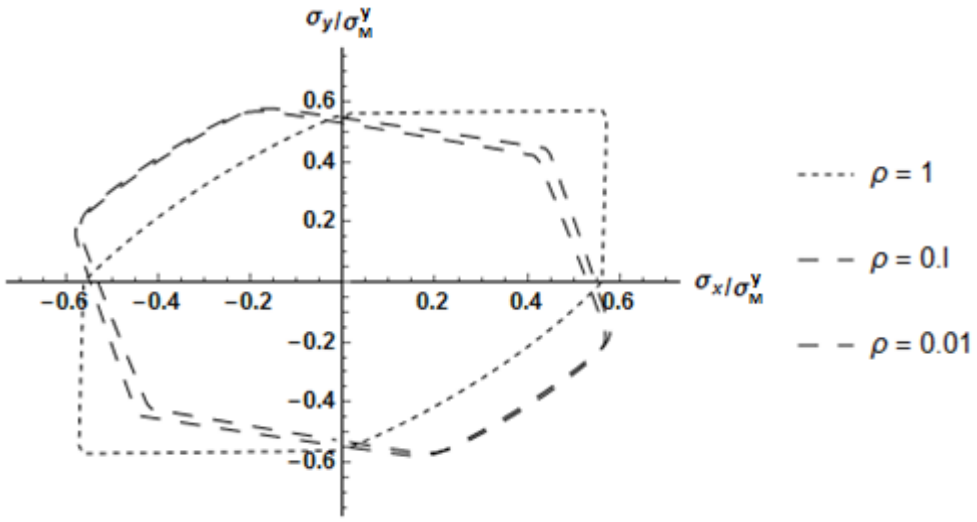

Figure 2-18 Effect of particle aspect ratio on the failure envelope of particulate reinforced composite materials under loading in the x-y plane.

The foregoing results were for loading in the x-y plane. Here the loading in the x-z plane will be examined. The axis, *Z,* is the axis of transverse isotropy of the composite material phases, the particles and matrix. Also it is the main axis of the prolate and oblate particles. Figures (2-21) and (2-22) show the failure envelope for three different fiber volume fractions, 5%, 10% and 30%. As expected, increasing the fiber volume fraction expands the failure envelopes. The composite material is weaker in the *z* direction .

Figure (2-22) compares the failure envelopes for various particle aspect ratios. Increasing the aspect ratio makes the composite material behave as transversely isotropic material. Spheres have less stress concentration than prolate particles in the *z* direction, therefore, composites having sphere particles show more strength.

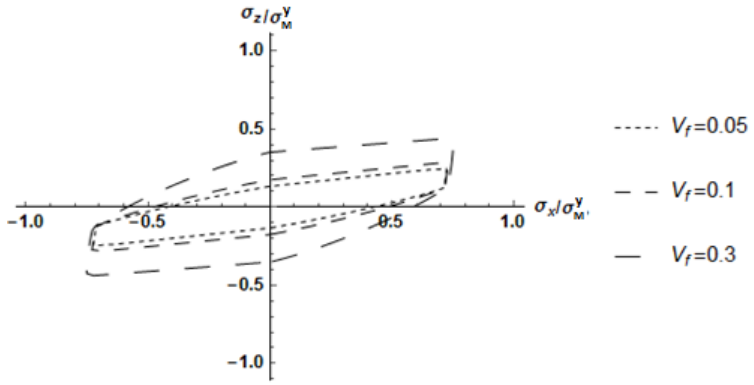

Figure 2-19 Failure envelope for a particulate reinforced composite embedding prolate ($\rho = 0.1$) reinforcing particles under loading in the x-z plane.

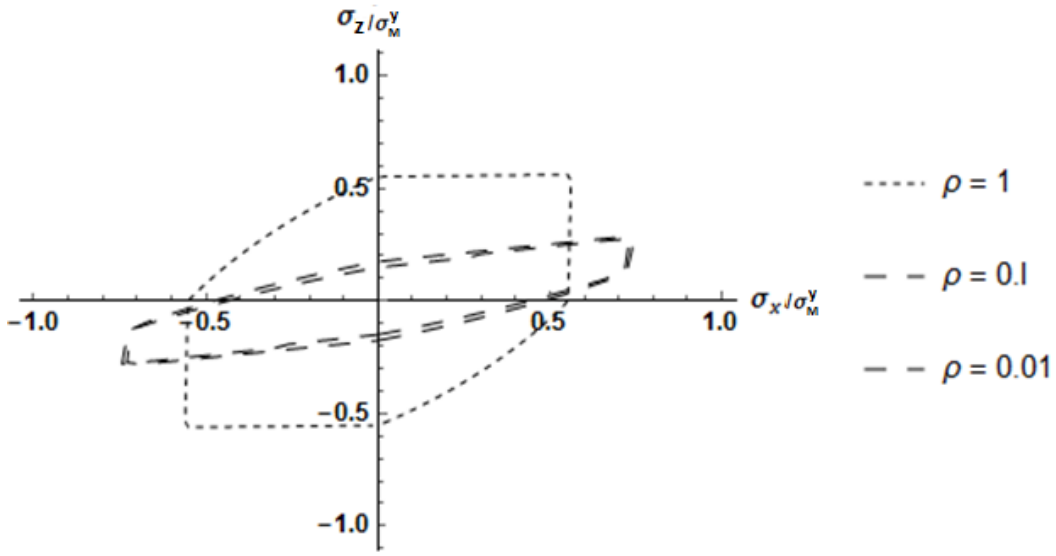

Figure 2-20 Comparison between the failure envelope of particulate reinforced composite for various particle aspect ratio under loading in the x-z plane.

2.5.4.2 Transversely isotropic matrix and particle

Figures (2-23) to (2-25) show the failure envelopes for particulate reinforced composites having a transversely isotropic matrix material. Qualitatively, these graphs are similar to the previously analyzed graphs for the isotropic matrix material and the graphs overall behavior are not a function of the anisotropy of the matrix material. Therefore, as expected, these graphs expand with increasing the particle volume fractions. Also Fig. (2-25) depicts the failure envelope in the x-z plane which embodies the axis of anisotropy. The composite material is weaker in the *z* direction due to the higher stress concentration values.

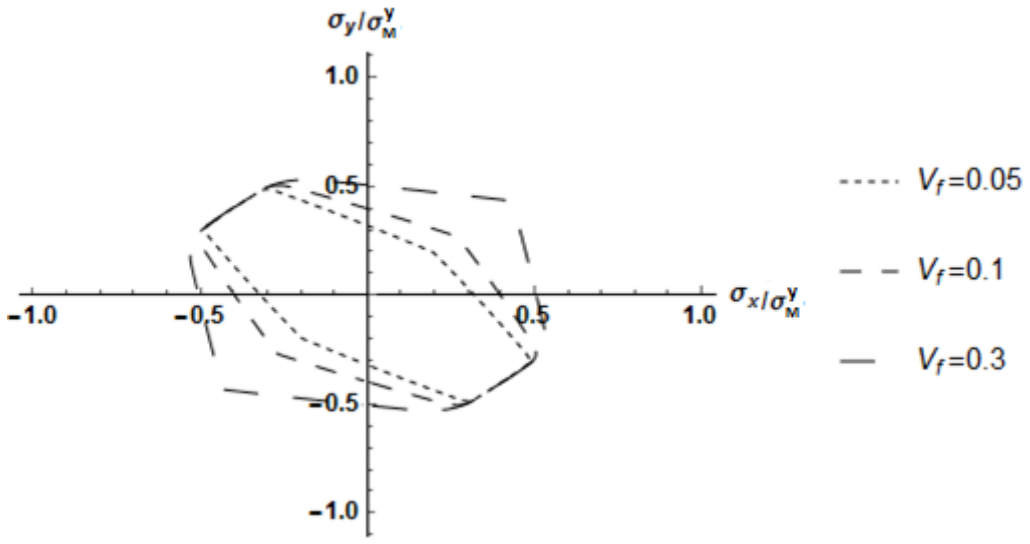

Figure 2-21 Failure envelope for transversely isotropic matrix phase reinforced with prolate particles under loading in the x-y plane.

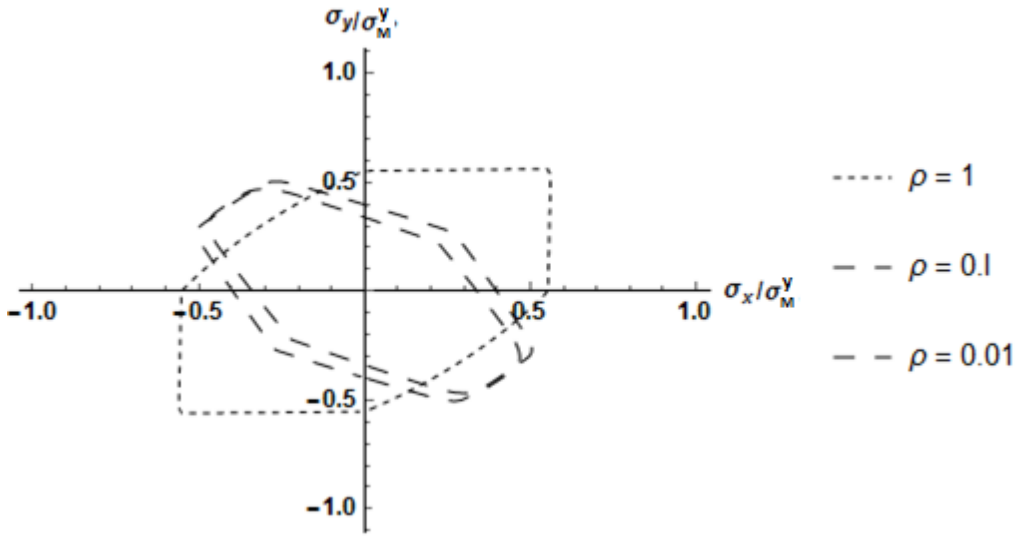

Figure 2-22 Failure envelope for transversely isotropic matrix phase reinforced with particles with various shapes.

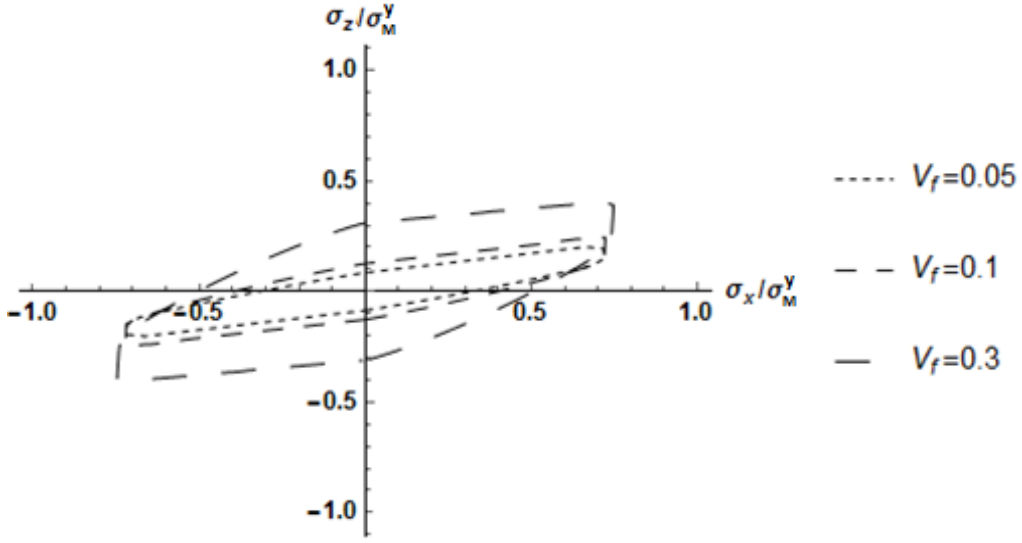

Figure 2-23 Failure envelope for transversely isotropic matrix phase reinforced with prolate particles under loading in the x-z plane.

Figure (2-26) shows the failure envelopes of particulate composite materials under shear loading for three values of fiber volume fraction, 5%, 10% and 30%. The particle aspect ratio is 0.01 which is a prolate sphere. Increasing the volume fraction expands the failure envelope graphs under normal stress direction but does not affect the strength under shear loading.

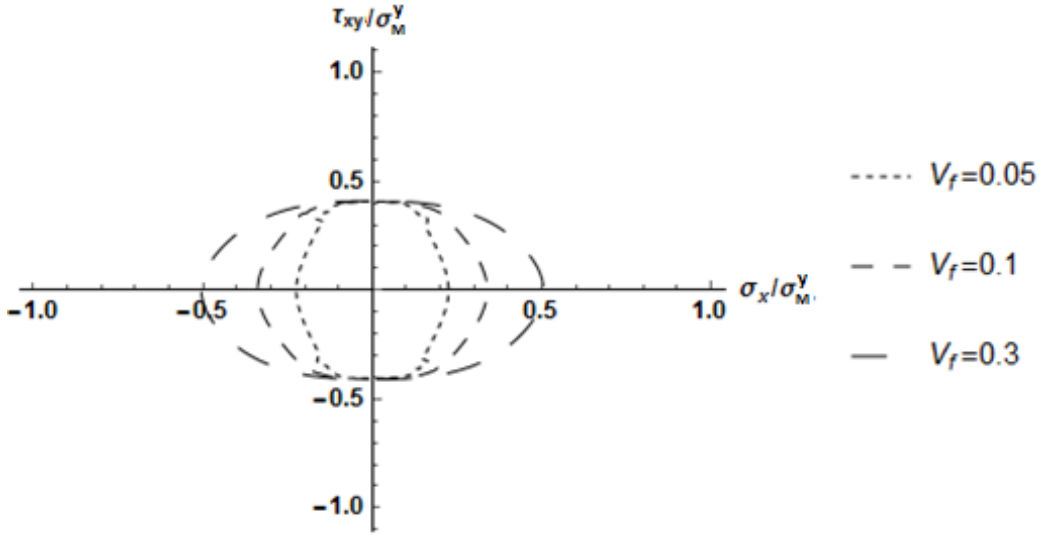

Figure 2-24 Failure envelope for transversely isotropic matrix phase reinforced with prolate particles under normal-shear loading in the x-y plane.

Figures (2-27) to (2-30) show the effect of the fiber volume fraction and particle aspect ratio on the S-C approximation of the stiffness tensor elements E_1, E_3, G_{12} and G_{13}. These elements are normalized with respect to the same properties of the matrix material. Increasing the fiber volume fraction increases the elastic stiffness tensor elements. The particle aspect ratio has various effects on the stiffness elements. Decreasing the particle aspect ratio increases the E_3 and G_{13} elements and decreases

the E_1 and G_{12} elements of the stiffness tensor. The particle aspect ratio has the lowest effect on the shear modulus in the x-z plane and it has the highest effect on the young's modulus in the z direction.

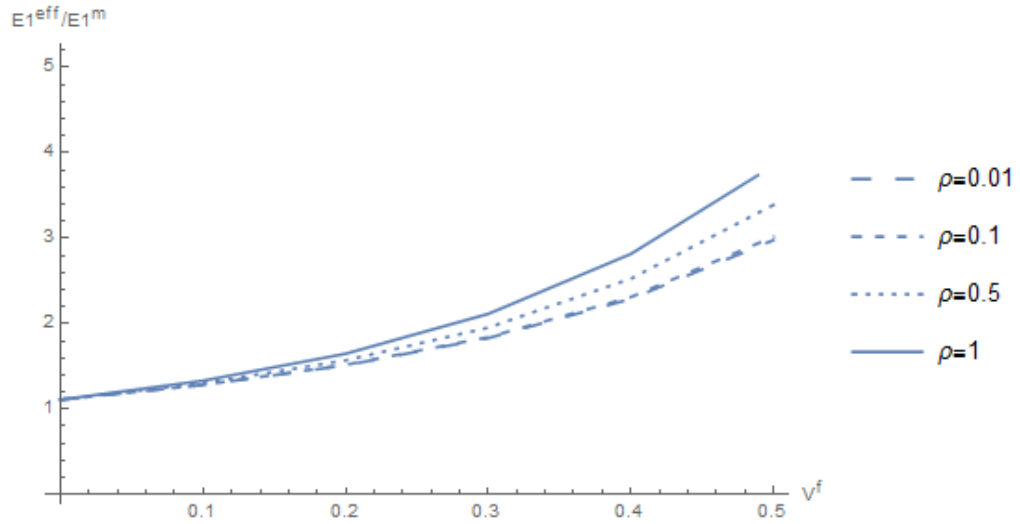

Figure 2-25 Effect of particle volume fraction and aspect ratio on the stiffness ratio, $\frac{E_1^{eff}}{E_1^m}$, of the S-C approximation of the composite material and pure matrix properties.

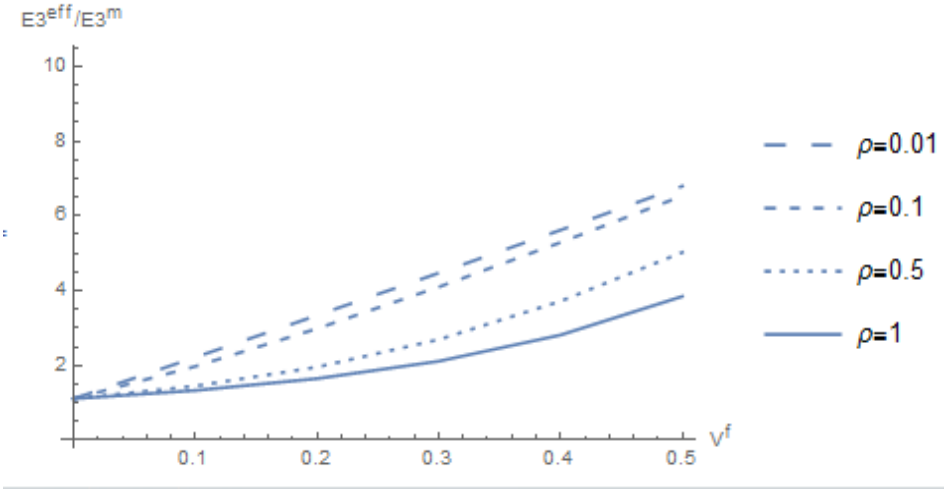

Figure 2-26 Effect of particle volume fraction and aspect ratio on the stiffness ratio, $\frac{E_3^{eff}}{E_3^m}$, of the S-C approximation of the composite material and pure matrix properties.

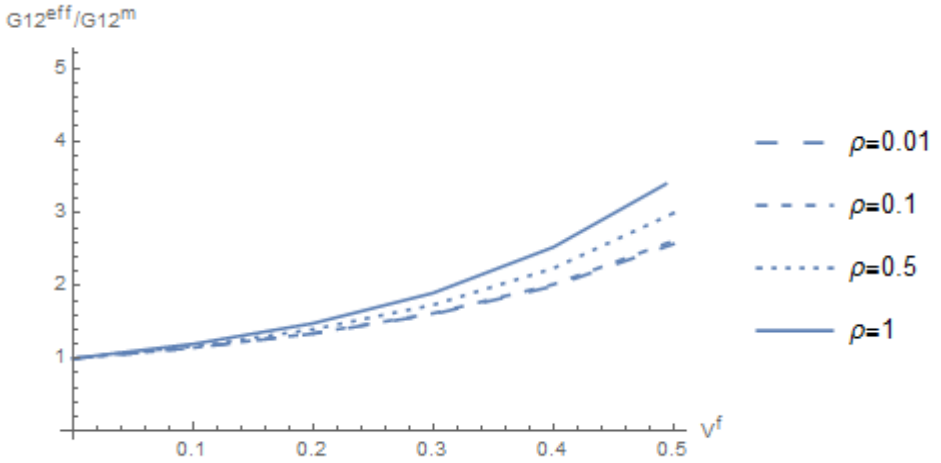

Figure 2-27 Effect of particle volume fraction and aspect ratio on the shear modulus ratio, $\frac{G_{12}^{eff}}{G_{12}^m}$, of the S-C approximation of the composite material and pure matrix properties.

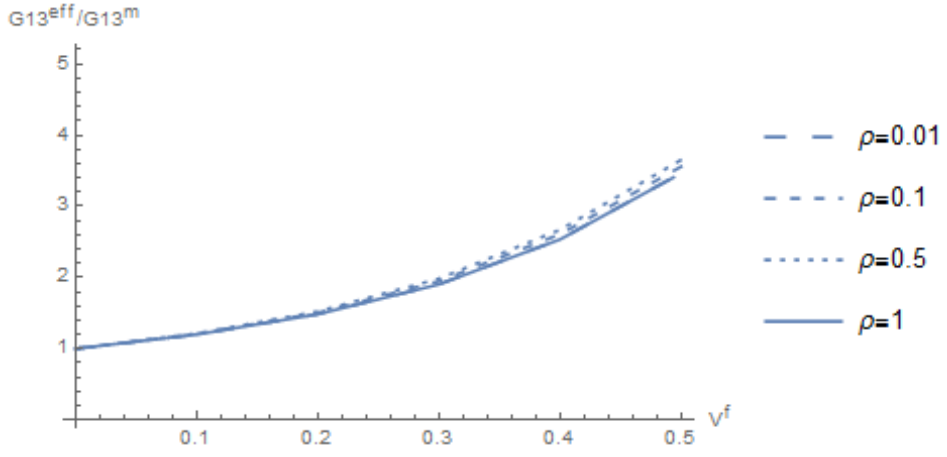

Figure 2-28 Effect of particle volume fraction and aspect ratio on the stiffness ratio, $\frac{G_{13}^{eff}}{G_{13}^{m}}$, of the S-C approximation of the composite material and pure matrix properties.

Chapter 3

Thermal Analysis

The particles in particulate reinforced composite materials have different thermal and elastic properties than the matrix. This causes localized thermal stresses under uniform heat flow at the far-field. Problems of such kind involve uncoupled thermo-elastic fields. This problem could be solved in two steps, first to obtain the temperature distribution, then the temperature field will be substituted into the thermo-elastic field and solved for the deformation and strain fields. Having the thermal stress field, the von Mises stress formula as a function of the applied far-field stress is obtained and maximized numerically to obtain the location where the maximum von Mises stress occurs. This stress value adds to the stress concentration due to mechanical loading and cause early yielding of the matrix material.

3.1 S-C approximation of effective thermal conductivity

The conductivity of composite materials as a whole is approximated using the self-consistent (S-C) approach. The phase components of composite materials are assumed to be homogeneous and isotropic. The quantities k_m and k_f are the constant thermal conductivities of the matrix and fibers, respectively. Assume that a two phase composite material is subjected to homogeneous heat flux boundary condition as

$$\lim_{r\to\infty} \nabla T = \nabla T^{\infty} = \theta_i \tag{3.1}$$

The heat flux, $\vec{q}$, in terms of the temperature gradient is defined as follows:

$$\overrightarrow{q_f} = -k_f \nabla T \tag{3.2}$$

$$\overrightarrow{q_m} = -k_m \nabla T \tag{3.3}$$

where "*T"* denotes the temperature distribution field. The effective thermal conductivity must be defined such that

$$\langle \vec{q} \rangle = -\bar{k} \langle \nabla T \rangle \tag{3.4}$$

where $\bar{k}$ is the S-C approximation of the composite material conductivity. It is well-known that for homogeneous material under uniform loading the average temperature gradient throughout the composite material is equal to the applied temperature gradient at the far-field.

$$\langle \nabla T \rangle = \nabla T^{\infty} = \theta_i \tag{3.5}$$

Therefore, substituting Eq. (3.5) into Eq. (3.4), results in

$$\langle \vec{q} \rangle = -\bar{k} \theta_i \tag{3.6}$$

also since the heat flux, $\vec{q}$, is piecewise continuous, therefore,

$$\langle \vec{q} \rangle = v_f \langle \vec{q} \rangle_f + v_m \langle \vec{q} \rangle_m \tag{3.7}$$

where $\langle \vec{q} \rangle_f$ and $\langle \vec{q} \rangle_m$ are the average heat flux in the fibers and matrix and v_f and v_m are the volume fraction of the fibers and matrix, respectively. Since each phase is homogenous and isotropic

$$\langle \vec{q} \rangle_m = -k_m \langle \nabla T \rangle_m \tag{3.8}$$

$$\langle \vec{q} \rangle_f = -k_f \langle \nabla T \rangle_f \tag{3.9}$$

Introducing Eqs. (3.8) and (3.9) into (3.7) yields

$$\bar{k}\theta_i = \upsilon_f k_f \langle \nabla T \rangle_f + \upsilon_m k_m \langle \nabla T \rangle_m \tag{3.10}$$

also we have

$$\theta_i = \upsilon_f \langle \nabla T \rangle_f + \upsilon_m \langle \nabla T \rangle_m \tag{3.11}$$

Elimination of $\langle \nabla T \rangle_m$ from Eq. (3.10) and (3.11) yields

$$\bar{k} = k_m + \upsilon_f \left(k_m - k_f\right) \frac{\langle \nabla T \rangle_f}{\theta_i} \tag{3.12}$$

This expression shows that the average of the temperature inside the particles is sufficient to evaluate the effective thermal conductivity.

3.2 S-C approximation of effective thermal expansion coefficient

The effective thermal expansion coefficient must be defined such that

$$\langle \epsilon_{ij} \rangle^T = \bar{\alpha} \delta_{ij} \langle T \rangle \tag{3.4}$$

where $\bar{\alpha}$ is the effective thermal expansion coefficient. The effective thermal expansion of the whole composite is evaluated using the S-C approximation approach. The derivation of this parameter was not the main purpose of this study, therefore, we obtained the explicit form from the review paper [30].

$$\bar{\alpha} = \alpha_m \left(1 - \nu_f\right) + \nu_f \alpha_f + \nu_f (1 - \nu_f)(\alpha_f - \alpha_m) \frac{\kappa_f - \bar{\kappa}}{\left(1 - \nu_f\right)\bar{\kappa} + \nu_f \kappa_f + \left(\frac{3\bar{\kappa}\kappa_f}{4\bar{\mu}}\right)} \tag{3.13}$$

where $\bar{\kappa}$ and $\bar{\mu}$ are the S-C approximation of the composite material bulk and shear modulus; which were explained thoroughly in the previous sections.

3.3 Temperature distribution

To obtain the temperature distribution field of a medium under a heat flow at the far-field, the Laplace equation must be solved. The Laplace equation and the boundary conditions are expressed as [31]:

$$\Delta T = 0 \tag{3.14}$$

$$\lim_{r\to\infty} T = \theta_k x_k \tag{3.15}$$

where θ_k is a constant temperature gradient in the "*k"* direction. The only possible format of the temperature distribution formula considering the heat flow at the far-field is expressed as follows:

$$T = f(r)\theta_k x_k \tag{3.16}$$

Substituting Eq. (3.16) into Eq. (3.14) yields

$$\Delta T = \left(f''(r) + \frac{4f'(r)}{r}\right)\theta_k x_k = 0 \tag{3.17}$$

Solving this differential equation yields $f(r)$ as

$$f(r) = \frac{C_1}{r^3} + C_2 \tag{3.18}$$

Therefore, the stress distribution is as follows:

$$T^f = (\frac{C_1}{r^3} + C_2)\theta_k x_k \tag{3.19}$$

$$T^m = (\frac{C_3}{r^3} + C_4)\theta_k x_k \tag{3.20}$$

The constants, C_1, C_2, C_3 and C_4, depend on the boundary conditions at the far-field and also at the interface. The quantities, T^f and T^m, are the temperature distribution inside the particles and matrix, respectively.

Since temperature inside the particles must remain finite, therefore, C_1 vanishes. Also at the far-field, the temperature gradient should be equal to θ_k, thus C_4 is equal to 1. Continuity condition for the temperature and heat flux at the particle-matrix interface yields C_2 and C_3. The temperature fields inside the particles and matrix are expressed as

$$T^f = \frac{3\bar{k}}{k_f + 2\bar{k}}\theta_k x_k \tag{3.21}$$

$$T^m = \left(-\frac{k_f - \bar{k}}{k_f + 2\bar{k}}\left(\frac{a}{r}\right)^3 + 1\right)\theta_k x_k \tag{3.22}$$

Having the temperature distribution, we could evaluate the S-C approximation of the effective conductivities. Substituting Eq. (3.21) into Eq. (3.11) and solving the resulted equations yield:

$$\bar{k} = \frac{1}{4}\left(2k_m - k_f - 3k_m\upsilon_f + 3k_f\upsilon_f + \sqrt{-24k_m(k_m - k_f)\upsilon_f + \left(k_f - 3k_f\upsilon_f + k_m(2 + 3\upsilon_f)\right)^2}\right) \tag{3.23}$$

3.4 Thermal stresses

Obtaining the thermal stresses inside the matrix and particles require solving the equilibrium equation. The general form of the equilibrium equation inside the matrix and particles is expressed as [31]

$$(C_{ijkl}u_{k,l})_{,j} - \left(C_{ijkl}\alpha\delta_{kl}\right)_{,j} = 0 \tag{3.24}$$

where α is the thermal expansion coefficient of the material. Substituting the explicit form of C_{ijkl} into Eq. (3.24) yields a simpler form as follows:

$$\mu u_{i,jj} + (\mu + \lambda)u_{j,ji} - (2\mu + 3\lambda)\alpha T_{,i} = 0 \tag{3.25}$$

where μ and λ are Lamé's constants. Using Eq. (3.21) and (3.22), the temperature gradient of the phases are as follows:

$$T_{,i}^{f} = \frac{3\bar{k}}{k_f + 2\bar{k}}\theta_i \tag{3.26}$$

$$T_{,i}^{m} = \left(1 + \frac{\bar{k} - k_f}{k_f + 2\bar{k}}\left(\frac{a}{r}\right)^3\right)\theta_i - \frac{3\left(\bar{k} - k_f\right)}{k_f + 2\bar{k}}\left(\frac{a}{r}\right)^3 \frac{x_k\theta_k x_i}{r^2} \tag{3.27}$$

Considering the form of the temperature gradients and equilibrium differential equation, the valid form of displacement , u_i, is expressed as

$$u_i = f(r)\ \theta_i + \frac{g(r)}{r^2}\theta_k x_k x_i \tag{3.28}$$

where $f(r)$ and $g(r)$ are to be determined for both phases separately. Substituting this relation into the equilibrium differential equation yields a system of differential equation as follow:

$$\begin{aligned}\left(\mu f''(r) + \frac{(\lambda+\mu)f'(r)}{r} + \frac{2\mu f'(r)}{r} + \frac{(\lambda+\mu)g'(r)}{r} + \frac{2g(r)(\lambda+\mu)}{r^2} + \frac{2\mu g(r)}{r^2}\right)\theta_i \\ + \left(\frac{(\lambda+\mu)f''(r)}{r^2} - \frac{(\lambda+\mu)f'(r)}{r^3} + \frac{(\lambda+\mu)g''(r)}{r^2} + \frac{\mu g''(r)}{r^2}\right. \\ \left. + \frac{(\lambda+\mu)g'(r)}{r^3} + \frac{2\mu g'(r)}{r^3} - \frac{4g(r)(\lambda+\mu)}{r^4} - \frac{6\mu g(r)}{r^4}\right)x_i\theta_i x_k \\ = (2\mu + 3\lambda)\alpha T_{,i}\end{aligned} \tag{3.29}$$

Solving for $f(r)$ and $g(r)$ for the matrix and particles yields some constants to be determined. Using the displacement and traction continuity conditions, finite deformation inside the particles and vanishing stress at the far-field, the remaining constants are obtained. In the case of the particles, the functions are as follow:

$$f(r) = c_1 - \frac{c_2}{3r^3} - \frac{c_3}{r} + \frac{r^2}{2}c_4 + \frac{k_m r^2 \alpha_f \left(12\lambda_f^2 + 35\lambda_f\mu_f + 18\mu_f^2\right)}{10\left(k_f + 2k_m\right)\mu_f\left(\lambda_f + 2\mu_f\right)} \tag{3.30}$$

$$g(r) = \frac{c_2}{r^3} - \frac{\lambda_f + \mu_f}{r\left(\lambda_f + 3\mu_f\right)}c_3 - \frac{r^2(\lambda_f + \mu_f)}{2\left(2\lambda_f + 3\mu_f\right)}c_4 + \frac{k_m r^2 \alpha_f \left(12\lambda_f^2 + 35\lambda_f\mu_f + 18\mu_f^2\right)}{10\left(k_f + 2k_m\right)\mu_f\left(\lambda_f + 2\mu_f\right)} \tag{3.31}$$

In the case of the matrix, the functions are as follow:

$$f(r) = d_1 - \frac{d_2}{3r^3} - \frac{d_3}{r} + \frac{r^2}{2}d_4 + \frac{\alpha_m(3\lambda_m + 2\mu_m)\left(5a^3\lambda_m\left(k_m - k_f\right) + r^3\left(k_f + 2k_m\right)(4\lambda_m + 9k_m)\right)}{30\,r\left(k_f + 2k_m\right)\mu_m(\lambda_m + 2\mu_m)} \tag{3.32}$$

$$g(r) = \frac{d_2}{r^3} - \frac{(\lambda_m + \mu_m)}{r(\lambda_m + 3\mu_m)}d_3 - \frac{r^2(\lambda_m + \mu_m)}{2(2\lambda_m + 3\mu_m)}d_4 - \frac{\alpha_m(3\lambda_m + 2\mu_m)\left(5a^3\left(k_f - k_m\right) + 2r^3\left(k_f + 2k_m\right)(\lambda_m + \mu_m)\right)}{30\,r\left(k_f + 2k_m\right)\mu_m(\lambda_m + 2\mu_m)} \tag{3.33}$$

The resulting stress outside the particle where the stress concentration occurs is expressed explicitly as follows:

$$A = (-15r^2\bar{\alpha}(6\bar{\lambda}^2 + 13\bar{\lambda}\bar{\mu} + 6\bar{\mu}^2)(-\bar{k} + k_f)(2\mu_f(4\bar{\mu} + \mu_f) \tag{3.34}$$
$$+ \lambda_f(2\bar{\mu} + 3\mu_f)) + a^2(\bar{\alpha}k_f(36\bar{\lambda}^2(\mu_f(3\lambda_f + 2\mu_f)$$
$$+ 5\bar{\mu}(\lambda_f + 4\mu_f)) + 5\bar{\lambda}\bar{\mu}(5\mu_f(3\lambda_f + 2\mu_f) + 78\bar{\mu}(\lambda_f$$
$$+ 4\mu_f)) + 2\bar{\mu}^2(-13\mu_f(3\lambda_f + 2\mu_f) + 90\bar{\mu}(\lambda_f$$
$$+ 4\mu_f))) + \bar{k}(90(2\bar{\lambda}^2 + 7\bar{\lambda}\bar{\mu} + 6\bar{\mu}^2)\alpha_f\mu_f(3\lambda_f + 2\mu_f)$$
$$- \bar{\alpha}(18\bar{\lambda}^2(11\mu_f(3\lambda_f + 2\mu_f) + 10\bar{\mu}(\lambda_f + 4\mu_f))$$
$$+ 5\bar{\lambda}\bar{\mu}(107\mu_f(3\lambda_f + 2\mu_f) + 78\bar{\mu}(\lambda_f + 4\mu_f))$$
$$+ 2\bar{\mu}^2(161\mu_f(3\lambda_f + 2\mu_f) + 90\bar{\mu}(\lambda_f + 4\mu_f))))))$$

$$B = r^2(-15r^2\bar{\alpha}(6\bar{\lambda}^2 + 13\bar{\lambda}\bar{\mu} + 6\bar{\mu}^2)(-\bar{k} + k_f)(2\mu_f(4\bar{\mu} + \mu_f) \tag{3.35}$$
$$+ \lambda_f(2\bar{\mu} + 3\mu_f)) + a^2(\bar{\alpha}k_f(36\bar{\lambda}^2(\mu_f(3\lambda_f + 2\mu_f)$$
$$+ 5\bar{\mu}(\lambda_f + 4\mu_f)) + 5\bar{\lambda}\bar{\mu}(5\mu_f(3\lambda_f + 2\mu_f) + 78\bar{\mu}(\lambda_f$$
$$+ 4\mu_f)) + 2\bar{\mu}^2(-13\mu_f(3\lambda_f + 2\mu_f) + 90\bar{\mu}(\lambda_f$$
$$+ 4\mu_f))) + \bar{k}(90(2\bar{\lambda}^2 + 7\bar{\lambda}\bar{\mu} + 6\bar{\mu}^2)\alpha_f\mu_f(3\lambda_f + 2\mu_f)$$
$$- \bar{\alpha}(18\bar{\lambda}^2(11\mu_f(3\lambda_f + 2\mu_f) + 10\bar{\mu}(\lambda_f + 4\mu_f))$$
$$+ 5\bar{\lambda}\bar{\mu}(107\mu_f(3\lambda_f + 2\mu_f) + 78\bar{\mu}(\lambda_f + 4\mu_f))$$
$$+ 2\bar{\mu}^2(161\mu_f(3\lambda_f + 2\mu_f) + 90\bar{\mu}(\lambda_f + 4\mu_f))))))$$

$$C = 5(9r^2\bar{\alpha}(6\bar{\lambda}^2 + 13\bar{\lambda}\bar{\mu} + 6\bar{\mu}^2)(-\bar{k} + k_f)(2\mu_f(4\bar{\mu} + \mu_f) + \lambda_f(2\bar{\mu} \quad (3.36)$$

$$+ 3\mu_f)) - a^2(\bar{\alpha}k_f(36\bar{\lambda}^2(\mu_f(3\lambda_f + 2\mu_f) + 5\bar{\mu}(\lambda_f$$

$$+ 4\mu_f)) + 5\bar{\lambda}\bar{\mu}(5\mu_f(3\lambda_f + 2\mu_f) + 78\bar{\mu}(\lambda_f + 4\mu_f))$$

$$+ 2\bar{\mu}^2(-13\mu_f(3\lambda_f + 2\mu_f) + 90\bar{\mu}(\lambda_f + 4\mu_f)))$$

$$+ \bar{k}(90(2\bar{\lambda}^2 + 7\bar{\lambda}\bar{\mu} + 6\bar{\mu}^2)\alpha_f\mu_f(3\lambda_f + 2\mu_f)$$

$$- \bar{\alpha}(18\bar{\lambda}^2(11\mu_f(3\lambda_f + 2\mu_f) + 10\bar{\mu}(\lambda_f + 4\mu_f))$$

$$+ 5\bar{\lambda}\bar{\mu}(107\mu_f(3\lambda_f + 2\mu_f) + 78\bar{\mu}(\lambda_f + 4\mu_f))$$

$$+ 2\bar{\mu}^2(161\mu_f(3\lambda_f + 2\mu_f) + 90\bar{\mu}(\lambda_f + 4\mu_f))))))$$

$$D = r^2(15r^2\bar{\alpha}(6\bar{\lambda}^2 + 13\bar{\lambda}\bar{\mu} + 6\bar{\mu}^2)(-\bar{k} + k_f)(2\mu_f(4\bar{\mu} + \mu_f) \quad (3.37)$$

$$+ \lambda_f(2\bar{\mu} + 3\mu_f)) + a^2(\bar{\alpha}k_f(36\bar{\lambda}^2(\mu_f(3\lambda_f + 2\mu_f)$$

$$+ 5\bar{\mu}(\lambda_f + 4\mu_f)) + 5\bar{\lambda}\bar{\mu}(5\mu_f(3\lambda_f + 2\mu_f) + 78\bar{\mu}(\lambda_f$$

$$+ 4\mu_f)) + 2\bar{\mu}^2(-13\mu_f(3\lambda_f + 2\mu_f) + 90\bar{\mu}(\lambda_f$$

$$+ 4\mu_f))) + \bar{k}(90(2\bar{\lambda}^2 + 7\bar{\lambda}\bar{\mu} + 6\bar{\mu}^2)\alpha_f\mu_f(3\lambda_f + 2\mu_f)$$

$$- \bar{\alpha}(18\bar{\lambda}^2(11\mu_f(3\lambda_f + 2\mu_f) + 10\bar{\mu}(\lambda_f + 4\mu_f))$$

$$+ 5\bar{\lambda}\bar{\mu}(107\mu_f(3\lambda_f + 2\mu_f) + 78\bar{\mu}(\lambda_f + 4\mu_f))$$

$$+ 2\bar{\mu}^2(161\mu_f(3\lambda_f + 2\mu_f) + 90\bar{\mu}(\lambda_f + 4\mu_f))))))$$

$$E = 15r^7(\bar{\lambda} + 2\bar{\mu})(2\bar{\lambda} + 3\bar{\mu})(2\bar{k} + k_f)(2\mu_f(4\bar{\mu} + \mu_f) + \lambda_f(2\bar{\mu} + 3\mu_f)) \quad (3.38)$$

$$\sigma_{ij}^{out} = \frac{A\, x_j\theta_i + Bx_i\theta_j + C\, x_ix_jx_p\theta_p + D\, x_p\theta_p\delta_{ij}}{E} \quad (3.39)$$

where the over-bar on the parameters denotes the S-C approximation. The tensor, σ_{ij}^{out} , is the stress outside the particles where the stress concentration is the highest.

Table 3-1 Average properties of usual reinforcing particles

	Al_2O_3	B_4C	SiC
Thermal Expansion [$\frac{\mu m}{m-c}$]	7.5	3.2	4
Thermal Conductivity [W/m-k]	25	17	120
Young's modulus [Gpa]	370	362	410

Table 3-2 Average properties of usual metal matrix

	Aluminum	Magnesium	Steel
Thermal Expansion [$\frac{\mu m}{m-c}$]	23	27	13
Thermal Conductivity [W/m-k]	205	100	40
Young's modulus [Gpa]	62	44	200

3.5 Results

Under a uniform heat flow at the far-field, particles inside a matrix with different thermal properties cause thermal stress concentrations. Based on the foregoing analysis, the stress field around a spherical particle is a function of the applied temperature gradient, θ_i, thermal properties and elastic properties of the composite material phases.

The von Mises stress distribution around the particles due to the thermal heat flow in the z and x direction at the far-field is illustrated in Figs. (3-1) and (3-2). The properties of aluminum as the matrix and alumina as the reinforcing particles are chosen from Tables (3-1) and (3-2). The temperature gradient is equal to $1\ [K/m]$ at the far-field. The stress distribution is a linear function of the thermal heat flow, therefore at higher thermal rates, the maximum von Mises stress is considerably large. Therefore, it is worthwhile to take a closer look at this phenomenon and effect of various parameters on the thermal stresses.

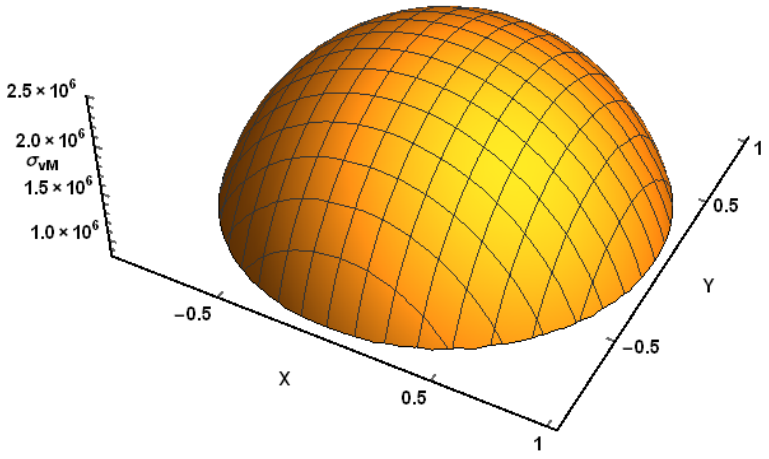

Figure 3-1 The von Mises stress distribution around particles in particulate reinforced composites under unit thermal heat flow in the z direction.

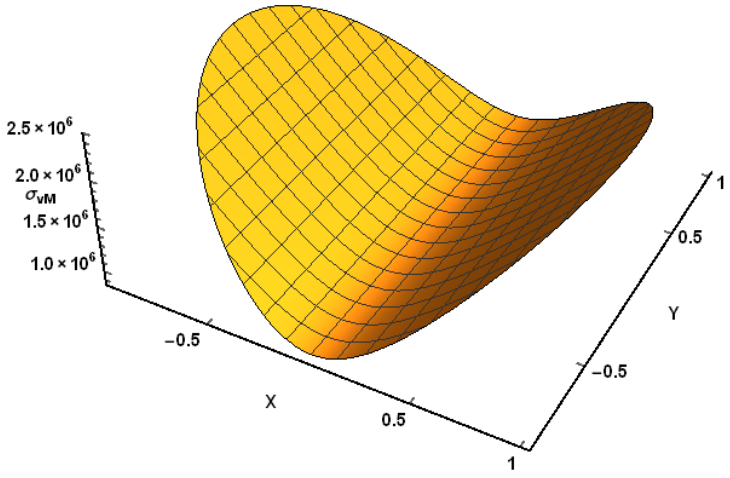

Figure 3-2 The von Mises stress distribution around particles in particulate reinforced composites under unit temperature gradient in the x direction.

The effect of fiber thermal expansion on the maximum von Mises stress is illustrated in Fig. (3-3). The maximum von Mises stress is normalized with respect to the temperature gradient at the far-field. The matrix is aluminum with thermal expansion equal to $23\ [\frac{\mu m}{m-c}]$. The fiber thermal expansion changes from 1 to 23. The maximum von Mises stress has the lowest value when the fiber thermal expansion coefficient is equal to $20\ [\frac{\mu m}{m-c}]$ which is lower than the matrix thermal expansion coefficient. This effect is due to the difference in conductivity of the two phases.

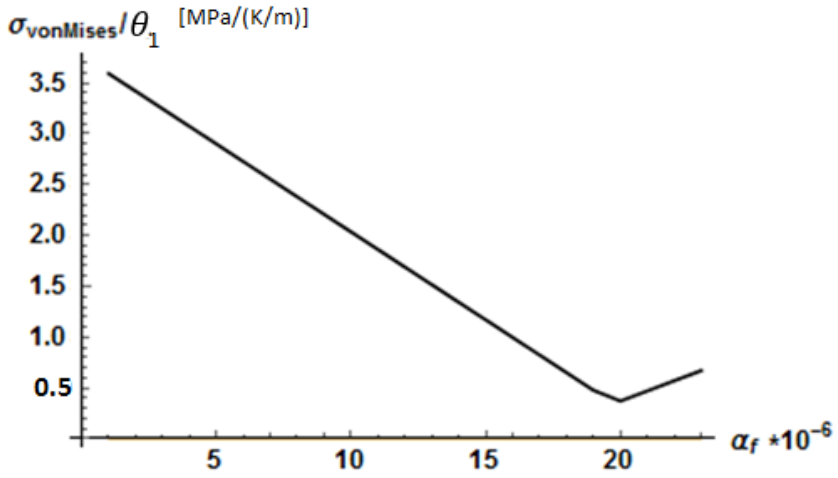

Figure 3-3 Effect of fiber thermal expansion coefficient on the maximum von Mises stress around fibers.

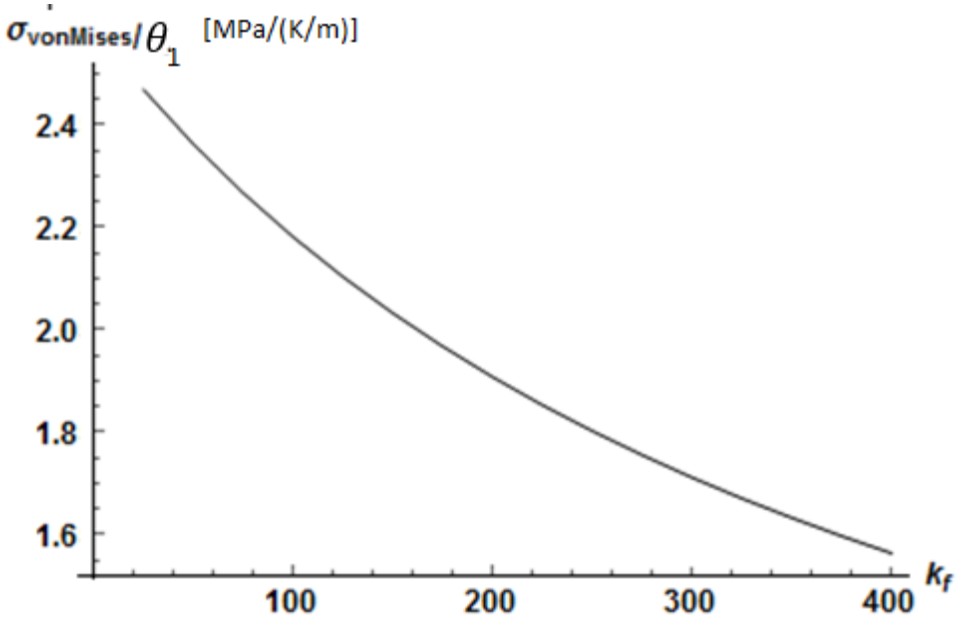

Figure 3-4 Effect of fiber thermal conductivity coefficient on the maximum von Mises stress around fibers.

Figure (3-4) depicts the effect of the fiber thermal conductivity on the maximum von Mises stress around the particle. Increasing the particle thermal conductivity coefficient decreases the maximum von Mises stress. The matrix thermal conductivity is equal to 205 [W/m-K]. If the phases have the same thermal conductivity, the temperature distribution will be uniform but due to the difference in thermal expansion, there will be stress in the medium.

The thermal conductivity and the thermal expansion coefficients are the two main parameters that affect the stress distribution inside a particulate reinforced composite under uniform heat flow at the far-field. Due to the symmetry of the geometry and applied loading, the failure envelopes are circular in 2-D. Therefore, investigating the effect of various parameters on the ultimate heat flow rate that causes yielding of the composite materials in terms of the magnitude of heat flow vector, $\|\vec{\theta}\|$, is sufficient.

Figure (3-5) depicts the ultimate far-field temperature gradient magnitude vs the particle volume fraction. The matrix is aluminum and the particles are alumina. The matrix yielding strength is 276 [Mpa]. Based on this graph, at a volume fraction equal to 0.05, the particulate reinforced composite could withstand approximately 115 [K/m] temperature gradient before yielding. Increasing the particle volume fraction, increases the ultimate far-field temperature gradient.

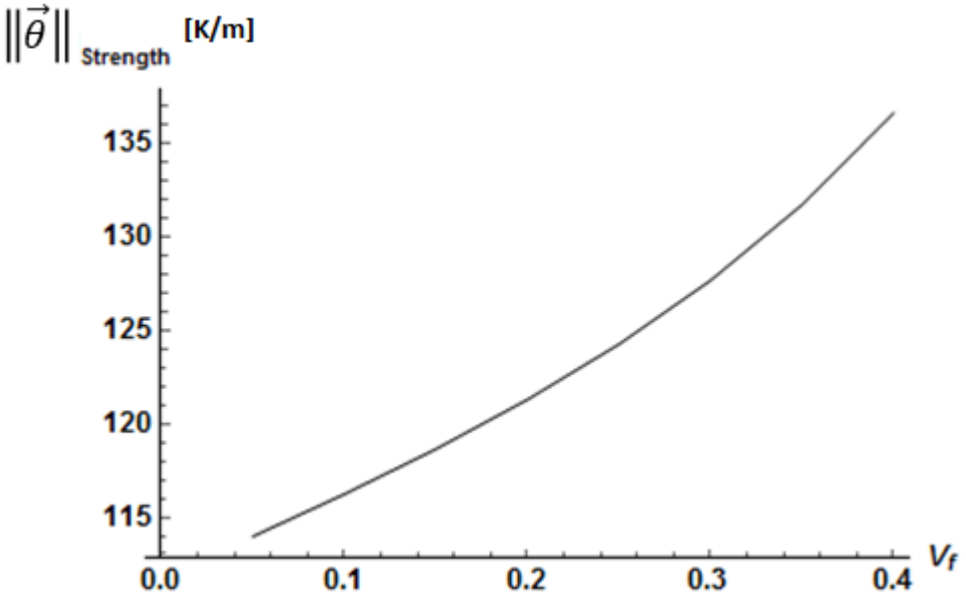

Figure 3-5 Ultimate far-field temperature gradient versus particle volume fractions.

Figure (3-6) illustrates the effect of fiber to matrix thermal expansion coefficient ratio on the ultimate far-field temperature gradient on aluminum/alumina particulate reinforced composite vs particle volume fraction. The behavior is not monotonic. At the lower ratios, increasing the particle volume fraction elevates the level of the ultimate far-field temperature gradient but at higher ratios, this behavior is reversed, i.e., increasing

the particle volume fraction causes a decrease in the ultimate far-field temperature gradient.

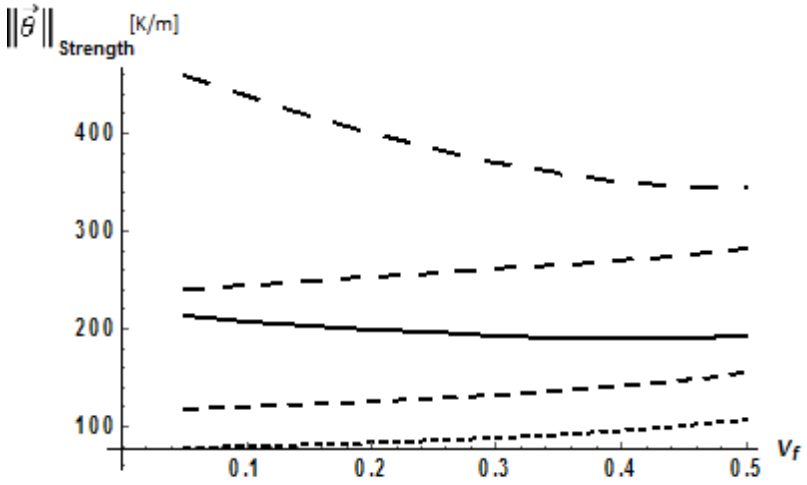

Figure 3-6 Ultimate far-field temperature gradient versus particle volume fraction for various particle to matrix thermal expansion ratios.

The effect of particle to matrix conductivity ratio on the ultimate far-field temperature gradient is illustrated in Fig. (3-7). This graph is for aluminum/alumina particulate reinforced composite. The particles conductivity is 25 [W/m-c] and the matrix conductivity is 205 [W/m-c]. Increasing the particles conductivity means changing the particle which will ultimately change the thermal expansion too. Therefore, studying the effect of thermal conductivity alone is not very practical but it is worthwhile to study this effect leaving thermal expansion coefficient constant. Increasing the thermal conductivity of the particles decreases the thermal stress distribution. This effect will ultimately increase the ultimate heat flow. Also, increasing the particle volume fraction monotonically increases the ultimate heat flow rate.

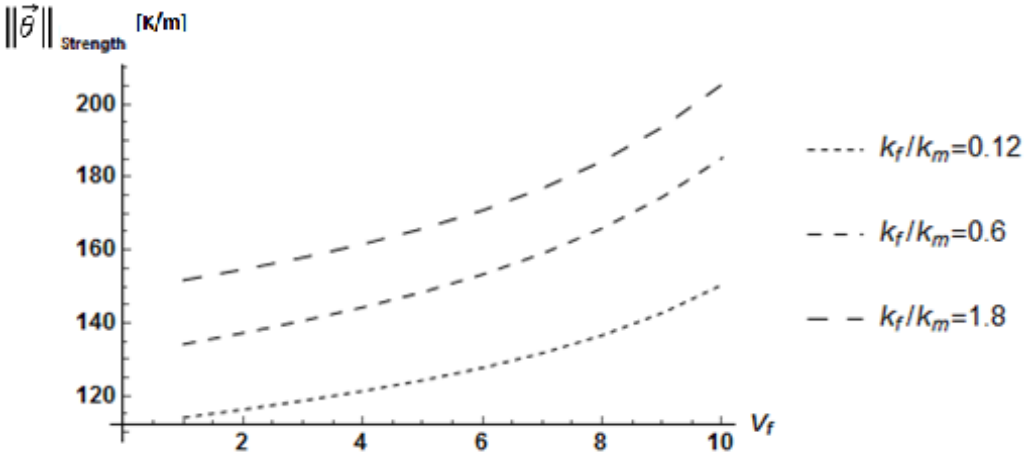

Figure 3-7 Ultimate far-field temperature gradient rate versus particle volume fraction for various particle to matrix conductivity ratios.

Chapter 4

Conclusion

Particulate composites span a large range of applications. Some everyday applications include automotive tires, concrete and dental amalgams. More advanced applications include artificial bone and metal cutting tools. Particulate composites are designed to satisfy specific performance requirements. Their performance is governed by the microstructure, interface, phase properties and fabrication. Among these factors, three of them could be analyzed theoretically to better optimize the composite to be more cost-effective. Fabrication could also be analyzed and optimized but is not in the scope of this dissertation. Therefore, developing theoretical formulation toward predicting the performance of these composite materials before manufacturing is highly desirable. An important aspect of any material during design phase is their strength under loading. Particulate composite materials strength has not been investigated as much as laminated composites have.

This dissertation attempted to step in the right direction toward predicting the strength of particulate composite materials using micromechanics of composite materials. Micromechanics of composite materials is more complicated compared to macromechanics but it brings forward a big advantage. Using micromechanics, the strength of the composite materials is predicted using the material and geometric properties of the phases which are available. Macromechanics requires various testing of each newly designed composite material prior to developing failure formulas.

The problem of strength of particulate composite materials is very complex, therefore simplified assumptions are necessary. It is assumed that the particles and matrix interface are perfectly connected, the particles have ellipsoidal shapes and the phases are linearly elastic transversely isotropic materials. The approach involves

replacing the composite materials containing a particle with the effective properties of the composite materials as a whole. The effective properties are obtained using a homogenization approach. In this study, we used the self-consistent approach due to its ability to simulate well beyond dilute particle distribution. The composite material surrounding a particle was replaced with the effective properties, the new problem is the same type as Eshelby's problem. Therefore, using the Eshelby tensor the uniform stress field inside the particles was evaluated as a function of the applied thermal or mechanical loading. The maximum von Mises stress happens on the particle-matrix interface outside the particles. To evaluate the stress field outside the particles, the traction and displacement continuity at the interface were utilized. The explicit form of the stress relation for specific case of spherical particles inside isotropic matrix is simple and was shown. But for a more general case of ellipsoidal particle inside transversely isotropic matrix, the explicit relation was too complex and long to show. Maximizing the von Mises stress field yields the location of the maximum von Mises stress and its value in terms of the applied loading. Substituting this value in the von Mises stress relation yields the ultimate thermal/mechanical loading that causes yielding of the matrix material. Through this procedure, the failure envelopes for various particulate composite materials were obtained. Also the effect of various parameters such as the particle volume fraction, particle to matrix stiffness ratio, thermal expansion ratio, thermal conductivity ratio and particle shape aspect ratio were studied thoroughly.

The stress distribution plots around cavity, rigid particle and elastic particles contain useful information that could help in understanding how the particle shape affects the yielding of the composite materials. The particle shapes are categorized into three main types, prolate spheroid, oblate spheroid and spheres. Under loading in the direction perpendicular to the isotropy plane, the von Mises stress concentration factor is highest if

the cavity is penny shaped. But in the case of rigid particles, the stress concentration factor is highest if the particle is needle shaped. The cases of cavity and rigid particles are two extreme cases of particles. In the case of having elastic particles, the behavior is more similar to rigid particles, i.e, the von Mises stress concentration factor is highest around prolate shaped particles.

The aforementioned information helps to understand the failure envelopes in two dimensions. Even though, the developed expressions for the failure criterion is not restricted to the biaxial case of loading, but the results were shown in a more customary 2-D failure envelopes. The 2-D plots of failure envelopes depict the ultimate far-field mechanical/thermal loading that would cause yielding of the matrix material. The failure envelope plots show that the strength of composite materials in yielding is lower than the strength of the pure matrix material. This happens due to the stress concentration around the particles. But yielding of the matrix material does not imply the ultimate yielding of the composite materials, it indicates the start of failure. The particles have other effects on the strength of the material as a whole. They obstruct the progress of cracks and also decrease the average stress inside the matrix material. Therefore, the failure process must be analyzed beyond yielding of the matrix material.

One of the shortcomings of the current study is the assumption that the fibers are all aligned in the same direction. Even though aligning the particles is not impossible to implement in practice, but a study should show their advantage over randomly aligned fibers. Therefore, studying the effect of fiber direction with respect to the material properties will be very helpful. Also this study investigated the elastic region of matrix material and determined the failure through the first point to yield. In practice yielding of an area rather than a point flags the failure. Therefore, to better predict the failure the analysis must include plastic deformation around the particles as well.

References

[1] Tsai, S. W., & Wu, E. M. (1972). A General Theory of Strength for Anisotropic Materials. doi:10.21236/ada306350.

[2] Christensen, R. M. (2005). *Mechanics of composite materials*. Mineola, NY: Dover.

[3] Tsai, S. W., & Hahn, H. T. (1980). *Introduction to composite materials*. Lancaster: Technomic Publ. Co.

[4] Ashbee, K. H. (1993). *Fundamental principles of fiber reinforced composites*. Lancaster: Technomic Publ.

[5] Argon, A. (1976). Stresses in and around slender elastic rods and platelets of different modulus in an infinite elastic medium under uniform. *Fibre Science and Technology, 9*(4), 265-275. doi:10.1016/0015-0568(76)90009-9.

[6] Benveniste, Y., & Aboudi, J. (1984). A continuum model for fiber reinforced materials with debonding. *International Journal of Solids and Structures, 20*(11-12), 935-951. doi:10.1016/0020-7683(84)90082-9.

[7] Mikata, Y., & Taya, M. (1985). Stress Field in a Coated Continuous Fiber Composite Subjected to Thermo-Mechanical Loadings. *Journal of Composite materials, 19*(6), 554-578. doi:10.1177/002199838501900607.

[8] Taya, M., & Chou, T. (1982). Prediction of the stress strain curve of a short-fibre reinforced thermoplastic. *Journal of Materials Science, 17*(10), 2801-2808. doi:10.1007/bf00644654.

[9] Reifsnider, K., Sendeckyj, G., Wang, S., Chiao, T., Johnson, W. S., Rodericks, G. Oshima, N. (1985). “A Method to Estimate the Overall Behavior of Fiber-Reinforced Hybrid Composites”., *Journal of Composites Technology and Research, 7*(3), 88. doi:10.1520/ctr10303j.

[10] Zhou, K., Hoh, H. J., Wang, X., Keer, L. M., Pang, J. H., Song, B., & Wang, Q. J. (2013). A review of recent works on inclusions. *Mechanics of Materials, 60*, 144-158. doi:10.1016/j.mechmat.2013.01.005.

[11] Hashin, Z., & Shtrikman, S. (1963). A variational approach to the theory of the elastic behaviour of multiphase materials. *Journal of the Mechanics and Physics of Solids, 11*(2), 127-140. doi:10.1016/0022-5096(63)90060-7.

[12] Nemat-Nasser, S. (1999). Averaging theorems in finite deformation plasticity. *Mechanics of Materials, 31*(8), 493-523. doi:10.1016/s0167-6636(98)00073-8.

[13] Budiansky, B. (1965). On the elastic moduli of some heterogeneous materials. *Journal of the Mechanics and Physics of Solids, 13*(4), 223-227. doi:10.1016/0022-5096(65)90011-6.

[14] Mori, T., & Tanaka, K. (1973). Average stress in matrix and average elastic energy of materials with misfitting inclusions. *Acta Metallurgica, 21*(5), 571-574. doi:10.1016/0001-6160(73)90064-3.

[15] Christensen, R., & Lo, K. (1979). Solutions for effective shear properties in three phase sphere and cylinder models. *Journal of the Mechanics and Physics of Solids, 27*(4), 315-330. doi:10.1016/0022-5096(79)90032-2.

[16] Zhang, G., & Wu, M. (2010). Connectivity and shape effects on the effective properties of piezoelectric–polymeric composites. *International Journal of Engineering Science, 48*(1), 37-51. doi:10.1016/j.ijengsci.2009.06.006.

[17] Paley, M., & Aboudi, J. (1992). Micromechanical analysis of composites by the generalized cells model. *Mechanics of Materials, 14*(2), 127-139. doi:10.1016/0167-6636(92)90010-b.

[18] Segurado, J., & Llorca, J. (2006). Computational micromechanics of composites: The effect of particle spatial distribution. *Mechanics of Materials, 38*(8-10), 873-883. doi:10.1016/j.mechmat.2005.06.026.

[19] Sozhamannan, G., Prabu, S. B., & Paskaramoorthy, R. (2010). Failures analysis of particle reinforced metal matrix composites by microstructure based models. *Materials & Design,31*(8), 3785-3790. doi:10.1016/j.matdes.2010.03.025.

[20] Lee, D. (2016). Fracture mechanical model for tensile strength of particle reinforced elastomeric composites. *Mechanics of Materials, 102*, 54-60. doi:10.1016/j.mechmat.2016.08.008.

[21] Kushch, V. (2003). Stress concentrations in the particulate composite with transversely isotropic phases. *International Journal of Solids and Structures, 40*(23), 6369-6388. doi:10.1016/s0020-7683(03)00399-8.

[22] Birman, V., Chandrashekhara, K., Hopkins, M., & Volz, J. (2013). Strength analysis of particulate polymers. *Composites Part B: Engineering, 54*, 278-288. doi:10.1016/j.compositesb.2013.05.009.

[23] Mori, T., & Tanaka, K. (1973). Average stress in matrix and average elastic energy of materials with misfitting inclusions. *Acta Metallurgica, 21*(5), 571-574. doi:10.1016/0001-6160(73)90064-3.

[24] Eshelby, J. D. The determination of the elastic field of an ellipsoidal inclusion, and related problems. *Solid Mechanics and its Applications Collected Works of J. D. Eshelby,* 209-229. doi:10.1007/1-4020-4499-2_18.

[25] Li, S., & Wang, G. (2017). *Introduction to micromechanics and nanomechanics*. New Jersey: World Scientific.

[26] Chou, T., Nomura, S., & Taya, M. (1980). A Self-Consistent Approach to the Elastic Stiffness of Short-Fiber Composites. *Journal of Composite materials, 14*(3), 178-188. doi:10.1177/002199838001400301.

[27] Withers, P. J. (1989). The determination of the elastic field of an ellipsoidal inclusion in a transversely isotropic medium, and its relevance to composite materials. *Philosophical Magazine A, 59*(4), 759-781. doi:10.1080/01418618908209819.

[28] Meng, C., Heltsley, W., & Pollard, D. D. (2012). Evaluation of the Eshelby solution for the ellipsoidal inclusion and heterogeneity. *Computers & Geosciences, 40*, 40-48. doi:10.1016/j.cageo.2011.07.008.

[29] Weinberger, CR, Cai, W, Barnett, DM. Elasticity of Microscopic Structures, ME340B Lecture Notes, Chapter 2, 2005, available at: http://micro.stanford.edu.ezproxy.uta.edu/~caiwei/me340b/content/me340b-notes_v01.pdf

[30] Sevostianov, I. (2012). On the thermal expansion of composite materials and cross-property connection between thermal expansion and thermal conductivity. *Mechanics of Materials, 45*, 20-33. doi:10.1016/j.mechmat.2011.10.001.

[31] Nomura, S. (2016). *Micromechanics with Mathematica*. Chicheter, West Sussex, United Kingdom: John Wiley & Sons.

Biographical Information

Behrooz Karimi received his bachelor's degree and master's degree from Iran University of Science and Technology and University of Tehran, respectively. His main focus was in computational mechanics. He received his doctorate from the University of Texas at Arlington for a dissertation about failure of particulate composite materials. During his doctorate degree, he was awarded Enhanced Graduate Teaching Assistantship.

His research interests include micromechanics and macromechanics of composite materials. He is also proficient in the finite element analysis of structural and thermal systems. He has worked on a several industrial projects including product design and development and also CAE software development.